

Searching for Relic Neutralinos using Neutrino Telescopes

V. Berezinsky^{a *}, A. Bottino^{b,c}, J. Ellis^d, N. Fornengo^{e,c}, G. Mignola^{d,c}
and S. Scopel^{f,g}

^a *INFN, Laboratori Nazionali del Gran Sasso, 67010 Assergi (AQ), Italy*

^b *Dipartimento di Fisica Teorica, Università di Torino, Via P. Giuria 1, 10125 Torino, Italy*

^c *INFN, Sezione di Torino, Via P. Giuria 1, 10125 Torino, Italy*

^d *Theoretical Physics Division, CERN, CH-1211 Geneva 23, Switzerland*

^e *Department of Physics and Astronomy, The Johns Hopkins University,
Baltimore, Maryland 21218, USA.*

^f *Dipartimento di Fisica, Università di Genova, Via Dodecaneso 33, 16146 Genova, Italy*

^g *INFN, Sezione di Genova, Via Dodecaneso 33, 16146 Genova, Italy*

Abstract

Neutrino telescopes of large area offer the possibility of searching for indirect signals of relic neutralinos in the galactic halo, due to annihilations in the Sun or the Earth. Here we investigate the sensitivity, using a supergravity scheme where the soft scalar mass terms are not constrained by universality conditions at the grand unification scale. We first discuss in which regions of the supersymmetric parameter space the neutralino may be considered as a good candidate for cold dark matter. The discovery potential of the search using neutrino telescopes is then compared to that of the direct search for relic neutralinos.

I. INTRODUCTION

In large regions of the supersymmetric parameter space the neutralino turns out to be the Lightest Supersymmetric Particle (LSP) and, as such, it is stable, provided R-parity is conserved. Under these hypotheses the neutralino would have decoupled from the initial plasma in the early stages of the Universe, and would now be present as a relic particle [1].

*E-mail: berezinsky@lngs.infn.it, bottino@to.infn.it, johne@cernvm.cern.ch,
fornengo@jhup.pha.jhu.edu, mignola@to.infn.it, scopel@ge.infn.it

The LSP is a candidate for the Cold Dark Matter (CDM) that is believed to have played a key role in the formation of structures in the Universe, such as galaxies and clusters. Although there are other candidates for CDM, such as the axion or the axino, and scenarios for structure formation that do not involve a large density of CDM, the possibility that the neutralino provides most of the CDM remains in our opinion the most attractive option. The “Standard Model” of structure formation used to be one with an initially flat Harrison-Zeldovich spectrum of inflationary fluctuations and (essentially) the critical density of CDM: $\Omega_{CDM} \equiv \rho_{CDM}/\rho_{crit} \simeq 1$. However, the advent of COBE and other data have suggested that this model needs to be modified, and there are three main contenders on the market [2].

One is a “Mixed” Dark Matter (or Cold Hot Dark Matter) model (CHDM), in which $\Omega_{CDM} \simeq 0.7$, there is a Hot Dark Matter component with $\Omega_{HDM} \simeq 0.2$, and baryons contribute $\Omega_B \lesssim 0.1$, as reviewed in Section 2. Another is a model (Λ CDM) with a significant cosmological constant $\Omega_\Lambda \simeq 0.7$ and $\Omega_{CDM} \simeq 0.3$. Finally, we mention a Cold Dark Matter with a tilted spectrum of initial fluctuations (TCDM), in which $\Omega_{CDM} \simeq 1$ is still possible, and an open model with $\Omega_{CDM} \simeq 0.3$. Calculations of the relic LSP abundance actually lead to values for the product $\Omega_{LSP}h^2$, where h is the present Hubble expansion rate H_0 in units of $100 \text{ Km} \cdot \text{s}^{-1} \cdot \text{Mpc}^{-1}$. There is still some observational uncertainty in this quantity, which may lie in the range $0.5 \lesssim h \lesssim 0.9$. Within this range, the age of the Universe favours smaller values of h in the CHDM and TCDM scenarios, whereas larger values are possible in the Λ CDM scenario. Combining the estimates of Ω_{CDM} and h in each of the three scenarios, we find the preferred range

$$\Omega_{CDM}h^2 = 0.2 \pm 0.1 \tag{1}$$

However, we repeat that not all the CDM need be constituted of LSPs, so Ω_{LSP} could in principle lie below the range (1).

Even if relic neutralinos do not provide a significant fraction of dark matter, experimental evidence for them would add a relevant new piece of information on the early stages of the Universe. Various strategies for detection of relic neutralinos are currently being pursued [3]. The most straightforward technique (direct detection) consists in measuring the effect that an impinging neutralino may produce in an appropriate detector by its elastic scattering off a target nucleus [4]. Among the indirect ways of detecting relic neutralinos, one of the most promising ones is the observation, using neutrino telescopes of large area, of the up-going muons which would be generated by neutrinos produced by pair annihilation of neutralinos captured and accumulated inside celestial bodies such as the Earth and the Sun [5–7].

At present, theory is unfortunately unable to offer firm predictions for the event rates for detection of relic neutralinos, since supersymmetric theories are still awaiting experimental verification. Only some hints for possible supersymmetric effects are available from accelerator data: supersymmetric theories would favor the unification feature of the gauge running constants [8] and the apparently relatively light Higgs boson mass [9]. Apart from these properties, the physical (correct) supersymmetric scheme is not known yet, and thus one has to consider a number of various possible scenarios. The detection rates for neutralinos depend very sensitively on the different supersymmetric schemes employed in the analysis.

The least constrained theoretical model is represented by the Minimal Supersymmetric extension of the Standard Model (MSSM), which incorporates the same gauge group as the

Standard Model and the minimal supersymmetric extension of its particle content [10]. The Higgs sector contains two doublets H_1, H_2 which give masses to down- and up-type quarks, respectively. This scheme provides a very useful framework for analyzing the phenomenology at the M_Z scale with a minimal number of model-dependent restrictions. The main inconvenience of this approach is that one typically has to deal with a large number of free parameters.

Much more ambitious are theoretical schemes where features at the M_Z scale are derived from properties at the Grand Unification (GU) scale (M_{GUT}), the link being provided by the Renormalization Group Equations (RGE's). One of the most attractive supersymmetric models is the one in which Electro-Weak Symmetry Breaking (EWSB) is induced radiatively [11]. This model is in no way the only possible model, but has the very nice feature of connecting the EWSB to soft supersymmetry breaking. Furthermore, the requirement of radiative EWSB is effective in reducing the number of the free parameters.

In order to constrain further the scheme, one often makes a number of rather restrictive hypotheses. Typically one assumes that not only the gauge couplings but also the Yukawa couplings of b and τ and the soft-breaking mass parameters (gaugino masses, scalar masses and trilinear couplings) unify at a GUT scale $M_{GUT} = O(10^{16} \text{ GeV})$. These assumptions entail very strong consequences for neutralino phenomenology, and in particular for the properties of neutralino dark matter. However, it has been shown that many aspects of neutralino phenomenology may change quite significantly, if one relaxes the universality requirements [12,13]. This possibility has been explored in Ref. [14] in an analysis of the neutralino relic abundance and of the event rates for direct detection in a wide range of the supersymmetric parameter space.

In the present paper we extend the analysis of Ref. [14] to the evaluation of the event rates for indirect relic neutralino searches using neutrino telescopes. Our results are compared with new, more stringent experimental bounds, obtained using the Baksan detector [15]. Furthermore, we also present a comparison between the discovery potential of searches using neutrino telescopes and the direct method.

The plan of the paper is as follows. In Sect. 2 we expand the above discussion of the CDM density, and derive the estimate (1) for $\Omega_{CDM}h^2$, by considering various cosmological models. The main features of the supersymmetric scheme employed in this paper are briefly described in Sect. 3, and in Sect. 4 we present our results on the neutralino relic abundance. Sect. 5 is devoted to the derivation of the flux of up-going muons due to neutralino-neutralino annihilation in the Earth and in the Sun. In Sect. 5 we also discuss some relevant features of the experimental layout required for the detection of the signals under study. Finally, results and conclusions are given in Sect. 6.

II. DENSITY OF CDM IN COSMOLOGICAL MODELS

Here we consider the neutralino as a CDM particle in the framework of several cosmological models. Such models are primarily characterized by two dimensionless parameters $h = H_0/(100 \text{ Km s}^{-1} \text{ Mpc}^{-1})$ and $\Omega = \rho/\rho_c$, where ρ is the relic cosmological density and $\rho_c \simeq 1.88 \cdot 10^{-29} h^2 \text{ g/cm}^3$ is the critical density.

Different measurements of the Hubble constant imply $0.4 \leq h \leq 1$ [16], but the recent measurements of extragalactic Cepheids in the Virgo [17] and Coma [18] clusters have narrowed this interval to $0.5 \lesssim h \lesssim 0.9$. However, this range should be taken with some caution, because of the uncertainties involved in these difficult measurements. In particular, the value $h = 0.5$ has to be considered as only marginally allowed. Inspired mostly by theoretical motivations (flatness problem and the beauty of the inflationary scenario), $\Omega = 1$ is usually assumed. This value is consistent with the IRAS [19] data and the POTENT [20] analysis, and no observational data contradict this value significantly.

Dark Matter can be subdivided into baryonic DM, hot DM (HDM) and CDM. The density of baryonic matter found from nucleosynthesis is taken [21] as $\Omega h^2 = 0.025 \pm 0.005$. The other DM components are defined as hot or cold components depending on their velocities at the moment when galaxies cross the horizon scale. If particles are relativistic they are called HDM particles, if not, CDM particles. The natural candidate for HDM is the heaviest neutrino, most probably the τ neutrino. Structure formation in the Universe puts strong restrictions to the properties of DM in the Universe. A Universe with only HDM and baryonic DM gives a wrong prediction for the spectrum of fluctuations as compared with the measurements of COBE [22], IRAS [19] and the CfA [23] survey. CDM and baryonic matter alone may explain the spectrum of fluctuations if the total density $\Omega \simeq 0.3$. There is one more possible form of energy density in the Universe, namely the vacuum energy described by the cosmological constant Λ . The corresponding energy density is given by $\Omega_\Lambda = \Lambda/(3H_0^2)$. Quasar lensing and the COBE results restrict the vacuum energy density to $\Omega_\Lambda \lesssim 0.7$.

There are several cosmological models based on the four types of DM described above (baryonic DM, HDM, CDM and vacuum energy). These models predict different spectra of fluctuations to be compared with the data of COBE, IRAS, the CfA survey, etc. They also produce different cluster-cluster correlations, number densities of clusters, velocity dispersions and other properties. The simplest and most attractive model for a correct description of all these phenomena is the mixed model (CHDM). This model is characterized by the following parameters:

$$\begin{aligned} \Omega_\Lambda = 0, \Omega_0 = \Omega_b + \Omega_{CDM} + \Omega_{HDM} = 1, \\ H_0 \simeq 50 \text{ Km s}^{-1} \text{ Mpc}^{-1} (h \simeq 0.5), \\ \Omega_{CDM} : \Omega_{HDM} : \Omega_b \simeq 0.7 : 0.2 : 0.1, \end{aligned} \tag{2}$$

where $\Omega_{HDM} \simeq 0.2$ is obtained in Ref. [24] from data on damped Lyman α clouds. In this CHDM model the central value for the CDM density is given by

$$\Omega_{CDM} h^2 = 0.18 \tag{3}$$

with uncertainties which may be estimated as $\lesssim \pm 0.1$. As already mentioned, the best candidate for the HDM particle is the τ neutrino, and in the CHDM model with $\Omega_\nu = 0.2$ its mass should be $m_{\nu_\tau} \simeq 4.7$ eV. A very good fit to the cosmological data is given by a CHDM model where the HDM is constituted of two neutrinos ($C\nu^2DM$ [25,26]). In our view, in either case, the most plausible candidate for the CDM particle is probably the neutralino (χ).

In the light of recent measurements of the Hubble constant, the CHDM model faces a possible *age problem*. A lower limit on the age of the Universe $t_0 \gtrsim 13$ Gyr from globular clusters imposes an upper limit on the Hubble constant in the CHDM model: $H_0 \lesssim 50 \text{ Km s}^{-1} \text{ Mpc}^{-1}$. This value is in slight contradiction with the recent observations of extragalactic Cepheids, which can be summarized as $H_0 \gtrsim 60 \text{ Km s}^{-1} \text{ Mpc}^{-1}$. However, it is too early to consider this as a serious conflict [27], if we take into account the many uncertainties and physical possibilities (e.g., the Universe can be locally overdense - see the discussion in ref. [26]).

The age problem, if taken seriously, can be solved with the help of another successful cosmological model, Λ CDM. This model assumes that $\Omega = 1$ is provided by the vacuum energy (cosmological constant Λ) and CDM. In this case we have $\Omega_\Lambda \simeq 0.7$, $\Omega_{CDM} \simeq 0.3$ and $h \lesssim 0.7$. Thus this model predicts $\Omega_{CDM}h^2 \simeq 0.15$ with an uncertainty of order 0.1.

Finally, we mention two other CDM models. The first one is the tilted CDM model (TCDM), where the initial fluctuation spectrum is steeper than the Harrison-Zeldovich spectrum, and the second one is the CDM model with $\Omega = \Omega_{CDM} = 0.3$ (CDM). Both models give a good fit to the observed spectrum of fluctuations as well as good agreement with the cluster data, though they may conflict with conventional inflationary prejudices.

In Table 1 we summarize the estimates of Ω_{CDM} for all these models and the ensuing values for $\Omega_{CDM}h^2$. Taking into account the uncertainties, we conclude as mentioned in

TABLE I. $\Omega_{CDM}h^2$ for five cosmological models

	Ω_{CDM}	h	$\Omega_{CDM}h^2$
CHDM	0.7	0.5	0.18
Λ CDM	0.3	0.7-0.8	0.15-0.19
$C\nu^2$ DM	0.7	0.5	0.18
TCDM	1.0	0.5	0.25
CDM	0.3	0.7-0.8	0.15-0.19

Sect. 1 that, for all the cosmological models considered here

$$\Omega_{CDM}h^2 = 0.2 \pm 0.1 \tag{4}$$

In the following we will emphasize regions of the supersymmetric parameter space which yield a neutralino relic abundance $\Omega_\chi h^2$ within the range of Eq.(4), but considering also regions with lower $\Omega_\chi h^2$, since there can be additional forms of CDM, such as axions.

III. THEORETICAL FRAMEWORK

We turn now to a short presentation of the theoretical model employed here to describe the neutralino. We adopt a supersymmetric model whose essential elements are provided by a Yang-Mills Lagrangian, the superpotential, which contains all the Yukawa interactions between the standard and supersymmetric fields, and by a soft-breaking Lagrangian with the usual trilinear couplings (with parameters A_i 's), the Higgs-mixing term μ , and the mass

terms (M_i for the gaugino masses and m_i for the scalar masses). While, for simplicity, unification conditions at M_{GUT} are imposed on gaugino masses: $M_i(M_{GUT}) \equiv m_{1/2}$, and for the trilinear couplings (A_0 being their common value at M_{GUT}), soft scalar masses are allowed to deviate from strict universality. More specifically, we consider here a departure from universality in the scalar masses at M_{GUT} that splits the soft-supersymmetry-breaking mass parameters of the two Higgs doublets M_{H_1} , M_{H_2} in the following way

$$M_{H_i}^2(M_{GUT}) = m_0^2(1 + \delta_i) . \quad (5)$$

The parameters δ_i are varied in the range $(-1, +1)$, but are taken to be independent of the other supersymmetric parameters.

Our supersymmetric parameter space is then constrained by a number of conditions: a) all experimental bounds on Higgs, neutralino, chargino and sfermion masses are satisfied (taking into account also the new data from LEP1.5 [28], b) the neutralino is the Lightest Supersymmetric Particle (LSP), c) constraints on the $b \rightarrow s\gamma$ process and on the mass of the bottom quark m_b assuming $b-\tau$ Yukawa unification are satisfied, d) EWSB is realized radiatively, e) radiative EWSB occurs without excessive fine-tuning, f) the neutralino relic abundance does not exceed the cosmological bound. In particular, the requirements of radiative EWSB and of the universality conditions on the gaugino masses and on the trilinear couplings allow a reduction of the independent parameters to the following set (apart from the δ_i 's): $m_{1/2}$, m_0 , A_0 , $\tan\beta$ ($\tan\beta$ is the ratio v_2/v_1 of the vacuum expectation values of the two Higgs doublets). It has to be emphasized that, because of the assumption of radiative EWSB, the parameter μ of the Higgs-mixing term in the superpotential is not a further independent parameter, but is a function of the previous set of parameters.

As we emphasized in our previous paper [14], attention must be paid to the condition that radiative EWSB is satisfied without excessive tuning [29,30]. In Ref. [14] we found that requiring accidental cancellations among various competing terms not to exceed the 1% level sets the bound $m_\chi \lesssim 200$ GeV. Further details of the theoretical scheme adopted here can be found in Ref. [14].

A departure from m_0 universality of the type given in Eq.(5) may modify the neutralino phenomenology in a significant way. Two key parameters whose values may change sizably, as functions of the δ_i 's, are μ and the mass m_A of the CP-odd Higgs boson A . In turn, variations in μ and M_A may induce significant modifications in the neutralino properties. It is convenient to express these two parameters in the following way [14]

$$\mu^2 = J_1 m_{1/2}^2 + J_2 m_0^2 + J_3 A_0^2 m_0^2 + J_4 A_0 m_0 m_{1/2} - \frac{M_Z^2}{2} \quad (6)$$

and

$$M_A^2 = K_1 m_{1/2}^2 + K_2 m_0^2 + K_3 A_0^2 m_0^2 + K_4 A_0 m_0 m_{1/2} - M_Z^2, \quad (7)$$

where the coefficients J_i and K_i , which are functions of $\tan\beta$ and of the δ_i (except for J_1 and K_1 which depend on $\tan\beta$ only), are obtained from the RGE's. The coefficients J_1 , J_2 and K_1 , K_2 are given in Fig. 1 for the case of m_0 universality. From now on we will set $A_0 = 0$, thus the other coefficients are irrelevant for our discussion. Except for very small values of $\tan\beta$ ($\tan\beta \lesssim 4$), one has $J_2 \ll J_1$, which in turn implies a strong $m_{1/2}-\mu$ correlation and

a gaugino-like neutralino. However, even moderate departures from m_0 universality may modify this picture [12,14]. For instance, at large $\tan\beta$, non vanishing values of the δ_i 's may yield a sizeable value of $|J_2|$, which in turn entails either a more pronounced gaugino-like neutralino, when $J_2 > 0$, or a mixed higgsino-gaugino composition for the neutralino, when $J_2 < 0$.

Also the coefficient K_2 plays a key role in establishing important phenomenological properties. In the universal case (see Fig.1), K_2 is positive and sizeable, except at very large $\tan\beta$ (*i.e.*, $\tan\beta \simeq 50$). Thus, M_A turns out to be large except at very large values of $\tan\beta$, where it may approach the present experimental bound $M_A \gtrsim 55$ GeV. Again, deviations from m_0 universality may modify K_2 substantially and thus may change the value of M_A , too. We will see in the following how these properties affect the values of some important quantities, such as the relic abundance.

For further details about the procedure we adopted to solve the RGE's and to implement the constraints due to $b \rightarrow s\gamma$ and to m_b , we refer to our previous paper [14]. Here we only recall that we used 1-loop beta functions including the whole supersymmetric particle spectrum from the GUT scale down to M_Z , neglecting the possible effects of intermediate thresholds. Two-loop and threshold effects, which are known to be of key importance for specific refined calculations, such as the unification of the gauge couplings, were not included, since we are interested in overall neutralino properties studied over a wide range of variation for the high-scale parameters. We have allowed generous ranges for $b \rightarrow s\gamma$ and m_b , to accommodate uncertainties in QCD corrections and the correct Yukawa unification condition, respectively. Furthermore, some physical solutions are unstable with respect to allowable variations in the strong gauge coupling constant α_s . Although the best way of proceeding would be to allow α_s to vary over its whole physical range, here, for simplicity, we have preferred to show our results only for some representative values of α_s . In one case in Sect. 4 we show comparatively our results for two different values of the strong coupling constant.

Our results for $\Omega_\chi h^2$ and for the detection rates have been obtained by varying the parameters m_0 and $m_{1/2}$ on an equally-spaced linear grid over the ranges $10 \text{ GeV} \leq m_0 \leq 2 \text{ TeV}$, $45 \text{ GeV} \leq m_{1/2} \leq 500 \text{ GeV}$ at fixed $\tan\beta$, with $A_0 = 0$. Furthermore, we remark that all evaluations presented here are for positive values of μ , since negative values of μ are disfavoured by the constraints due to m_b and the $b \rightarrow s\gamma$ process.

As far as the values of $\tan\beta$ are concerned, we note that recent global fits of the electroweak data within the MSSM [31] focused interest on two narrow intervals for $\tan\beta$: (i) very small values, $\tan\beta \simeq 1 - 2$ (*i.e.*, close to the quasi-infrared fixed point for a given value of m_t), or (ii) very large values of $\tan\beta$ (*i.e.*, of order m_t/m_b). In the present paper, as representative values for case (i) and case (ii), we take the values $\tan\beta = 1.5$ and $\tan\beta = 53$, respectively.

We conclude this section by summarizing the basic features of our model [14]: (i) the universality condition for the scalar masses is relaxed, (ii) rather relaxed restrictions from $b \rightarrow s\gamma$ and the mass of the b quark are allowed, (iii) the fine-tuning condition limits the neutralino mass to $m_\chi \lesssim 200$ GeV.

IV. NEUTRALINO RELIC ABUNDANCE

For the evaluation of $\Omega_\chi h^2$ we have followed the standard method [32–35]. We recall that $\Omega_\chi h^2$ is essentially given by $\Omega_\chi h^2 \propto \langle \sigma_{\text{ann}} v \rangle_{\text{int}}^{-1}$, where $\langle \sigma_{\text{ann}} v \rangle_{\text{int}}$ is the thermally-averaged annihilation cross section, integrated from the freeze-out temperature to the present temperature. Then the key quantity to be evaluated is the annihilation cross-section.

In the evaluation of σ_{ann} we have considered the following set of final states: (1) fermion-antifermion pairs, (2) pairs of charged Higgs bosons, (3) one Higgs boson and one gauge boson, (5) pairs of gauge bosons. For the final state (1), the following diagrams have been considered: Higgs- and Z-exchange diagrams in the s channel and \tilde{f} exchange in the t channel. For the final states (2 to 5) we have included Higgs-exchange and Z-exchange diagrams in the s channel, and either neutralino (the full set of the four mass eigenstates) or chargino exchange in the t channel, depending on the electric charges of the final particles [35].

The relative importances of the various exchange diagrams depend on the supersymmetric parameters through the couplings and masses of the exchanged particles. Typically, one expects a small value of σ_{ann} at small $\tan\beta$, where σ_{ann} is dominated by sfermion and Z exchanges. In fact, in supergravity models at small $\tan\beta$, Higgs-exchange contributions are reduced not only by small couplings, but also by large values of the mass M_A . These features are displayed in Fig. 2, which is for $\tan\beta = 1.5$ and $\delta_1 = \delta_2 = 0$. As expected, $\Omega_\chi h^2$ is rather large, and many configurations are excluded by the cosmological bound $\Omega h^2 \leq 1$. The allowed region (denoted by squares) is mainly due to configurations where σ_{ann} is dominated by \tilde{l} exchange. Filled diamonds denote configurations where $\Omega_\chi h^2$ is in the range of Eq.(4). In these configurations typical values for the mass parameters are: $m_{\tilde{l}} \simeq (150 - 200)$ GeV, $m_{\tilde{q}} \gtrsim 600$ GeV, $M_A \simeq 1$ TeV. In Fig. 2(b) we notice that the allowed domain extends to the right of the line $m_0 = m_{0,\text{min}}$ (where $m_{0,\text{min}}$ is the minimal value for m_0), allowing for the neutralino only a gaugino-dominated region. This occurs because the coefficient J_2 of Eq.(6) is positive (see Fig.1).

An illustration of how a deviation from m_0 universality may somewhat modify the picture is provided by Fig. 3, where we display the relevant physical regions when we choose a departure from universality: $\delta_1 = -1.0, \delta_2 = 1.0$, which makes the coefficient J_2 very small and negative. As a consequence, $m_{1/2}$ and μ are strongly correlated, with a slight extension of the neutralino physical region toward the sector of higgsino-gaugino mixture for $m_{1/2} \gtrsim 400$ GeV (see Fig. 3(b)). These new configurations, which turn out to correspond to high values of m_0 : $m_0 \simeq (1.3 - 1.6)$ TeV, are no longer in conflict with the cosmological bound, at variance with the universal case. In these points of the parameter space σ_{ann} is dominated by the \tilde{t} -exchange, since here $m_{\tilde{t}} \simeq 250$ GeV. However, we remark that these configurations realize radiative EWSB only with strong fine tuning. The generic trend is to have, for $\delta_1 = -1.0, \delta_2 = 1.0$, $\Omega_\chi h^2$ smaller than in the universal case and this feature is displayed in Fig. 3, where we notice that the cosmological constraint is less effective here in restricting the parameter space, as compared to the universal case (see Fig. 2).

Let us turn now to large values of $\tan\beta$. As was already pointed out in Ref. [14] for the universal case at $\tan\beta = 53$, the neutralino relic abundance is very low: $\Omega_\chi h^2 \lesssim 0.1$, due to small values of M_A : $M_A \lesssim 150$ GeV, which generates a large σ_{ann} dominated by

Higgs-exchange contributions.

By moving away from m_0 universality, we can change the picture noticeably. For instance, by taking $\delta_1 = 0.4, \delta_2 = -0.1$, we can generate large values of $\Omega_\chi h^2$. However, as we see in Fig. 4, most of the configurations of large $\Omega_\chi h^2$ are disallowed by the constraint on the bottom mass (and also marginally by the constraint $b \rightarrow s\gamma$). The reason for the marked difference between this case and the universal one is that now M_A is large. Indeed, the lowest allowed values of M_A ($M_A \simeq 150$ GeV) only occur in the parameter region: $m_0 \simeq 300$ GeV, $m_{1/2} \simeq 400$ GeV. The large values of M_A are caused by a sizeable, positive value for the coefficient K_2 of Eq.(7). The only allowed configurations which provide $\Omega_\chi h^2$ in the range of Eq.(4) are those with $m_{1/2} \simeq 120$ GeV and 1.2 TeV $\lesssim m_0 \lesssim 1.8$ TeV. Notice that some of these configurations do not satisfy our no-fine-tuning constraint. The relevance of the α_s value in determining $\Omega_\chi h^2$ and in shaping the allowed physical regions is apparent when Fig. 4, evaluated for $\alpha_s = 0.1127$, is compared to Fig. 5, evaluated for $\alpha_s = 0.118$.

V. EVALUATION OF THE SIGNALS

As was anticipated in the Introduction, the signals to be discussed in the present paper consist of the fluxes of up-going muons through a neutrino telescope generated by neutrinos which are produced by pair annihilations of neutralinos captured and accumulated inside the Earth and the Sun. The steps involved in this process are the following: a) capture by the celestial body of the relic neutralinos through a slow-down process due essentially to neutralino elastic scattering off the nuclei of the macroscopic body, b) accumulation of the captured neutralinos in the central part of the celestial body, c) neutralino-neutralino annihilation with emission of neutrinos, and for the various annihilation products, d) propagation of neutrinos and conversion of their ν_μ component into muons in the rock surrounding the detector (or, much less efficiently, inside the detector), and finally e) propagation and detection of the ensuing up-going muons in the detector.

The various quantities relevant for the previous steps are calculated here according to the method described in Ref. [6], to which we refer for further details.

A. Neutralino local density

As will be shown explicitly in the subsequent subsection, the capture rate of the relic neutralinos is proportional to the local neutralino density ρ_χ in the solar neighbourhood. Let us specify here how ρ_χ is evaluated.

For each point of the model parameter space we first calculate the relevant value of the cosmological neutralino relic density according to the procedure outlined in Sect. 4. Whenever $\Omega_\chi h^2$ is larger than a minimal $(\Omega h^2)_{\min}$ suggested by observational data and by large scale structure calculations, we simply put $\rho_\chi = \rho_l$, where ρ_l is the local halo density. In the points of the parameter space where $\Omega_\chi h^2$ is less than $(\Omega h^2)_{\min}$, the neutralino may only provide a fractional contribution $\Omega_\chi h^2 / (\Omega h^2)_{\min} \equiv \xi$ to Ωh^2 ; in this case we take $\rho_\chi = \rho_l \xi$. The value to be assigned to $(\Omega h^2)_{\min}$ is somewhat arbitrary. Here it is set equal to 0.1. As far as the local halo density ρ_l is concerned, we are inspired by the recent estimate $\rho_l = 0.51^{+0.21}_{-0.17}$ GeV cm⁻³ [36], based on a flattened dark matter distribution and recent microlensing data.

This introduces a significantly larger central value as compared to previous determinations (see, for instance, Ref. [37]). All the numerical results presented in this paper were obtained using the value $\rho_l = 0.5 \text{ GeV cm}^{-3}$.

B. Capture rates and annihilation rates

For the evaluation of the capture rate C of the relic neutralinos by a celestial body we have used the standard formula [38]

$$C = \frac{\rho_\chi}{v_\chi} \sum_i \frac{\sigma_i}{m_\chi m_i} (M_B f_i) \langle v_{esc}^2 \rangle X_i, \quad (8)$$

where v_χ is the neutralino mean velocity, σ_i is the cross section of the neutralino elastic scattering off the nucleus i of mass m_i , $M_B f_i$ is the total mass of the element i in the body of mass M_B , $\langle v_{esc}^2 \rangle_i$ is the square escape velocity averaged over the distribution of the element i , and X_i is a factor which takes account of kinematical properties occurring in the neutralino–nucleus interactions. For the evaluation of the elastic χ –nucleus cross sections we refer to [14].

The annihilation rate Γ_A of the neutralinos inside the macroscopic body is calculated with the formula [39]

$$\Gamma_A = \frac{C}{2} \tanh^2 \left(\frac{t}{\tau_A} \right) \quad (9)$$

where t is the age of the macroscopic body ($t = 4.5 \text{ Gyr}$ for Sun and Earth), $\tau_A = (CC_A)^{-1/2}$, and C_A is the annihilation rate per effective volume of the body, given by

$$C_A = \frac{\langle \sigma v \rangle}{V_0} \left(\frac{m_\chi}{20 \text{ GeV}} \right)^{3/2} \quad (10)$$

Here, V_0 is defined as $V_0 = (3m_{pl}^2 T / (2\rho \times 10 \text{ GeV}))^{3/2}$ where T and ρ are the central temperature and the central density of the celestial body. For the Earth ($T = 6000 \text{ K}$, $\rho = 13 \text{ g} \cdot \text{cm}^{-3}$) $V_0 = 2.3 \times 10^{25} \text{ cm}^3$, for the Sun ($T = 1.4 \times 10^7 \text{ K}$, $\rho = 150 \text{ g} \cdot \text{cm}^{-3}$) $V_0 = 6.6 \times 10^{28} \text{ cm}^3$. Also, σ_{ann} is the neutralino–neutralino annihilation cross section and v is the relative velocity: $\langle \sigma_{\text{ann}} v \rangle$ is calculated with all the contributions at the tree level as previously discussed in Sect. 4, with the further inclusion here of the two–gluon annihilation final state [40].

From Eq.(9) it follows that in a given macroscopic body the equilibrium between capture and annihilation (*i.e.* $\Gamma_A \sim C/2$) is established only when $t \gtrsim \tau_A$. We stress here that the neutralino density ρ_χ enters not only in C but also in τ_A (through C). Thus, the use of a correct value for ρ_χ (rescaled, when necessary) is important also in determining whether or not equilibrium is reached in a macroscopic body.

From the evaluation of the annihilation rate for neutralinos inside the Earth and the Sun it turns out that, for the Earth, the equilibrium condition depends sensitively on the values of the model parameters, and is not satisfied in wide regions of the parameter space. Consequently, for these regions the signal due to neutralino annihilation may be significantly

attenuated. On the contrary, in the case of the Sun, equilibrium between capture and annihilation is reached for the whole range of m_χ , due to the much more efficient capture rate due to the stronger gravitational field [38].

C. Neutrino fluxes

Let us turn now to the evaluation of the neutrino fluxes due to the annihilation processes taking place in the celestial bodies. For a distant source such as the Sun the differential rate in the neutrino energy E_ν is given by

$$\frac{dN_\nu}{dE_\nu} = \frac{\Gamma_A}{4\pi d^2} \sum_{F,f} B_{\chi f}^{(F)} \frac{dN_{f\nu}}{dE_\nu} \quad (11)$$

where d is the distance from the source, F denotes the χ - χ annihilation final states, $B_{\chi f}^{(F)}$ denotes the branching ratios into heavy quarks, τ leptons and gluons in the channel F ; $dN_{f\nu}/dE_\nu$ is the differential distribution of the neutrinos generated by the hadronization of quarks and gluons and the subsequent hadronic semileptonic decays.

In the case of the Earth one has to take into account the size of the region around the center of the Earth where most of the neutralinos are accumulated. This is important, since the angular dependence of the flux plays a crucial role in providing a signature, and, potentially, in allowing a determination of the neutralino mass [38,6,41]. For details about the relevant formulae we refer to [6]. Here we only give some information about our evaluation of the spectrum $dN_{f\nu}/dE_\nu$ to be employed in Eq.(11). The neutrino spectra due to b and c quarks, τ leptons and gluons were computed using the Jetset 7.2 Monte Carlo code [42]. We have neglected the contributions of the light quarks directly produced in the annihilation process or in the hadronization of heavy quarks and gluons, because these light particles stop inside the medium (Sun or Earth) before their decay [43]. For the case of the Sun we have also considered the energy loss of the heavy hadrons in the solar medium. The spectra due to heavier final states, *i.e.* Higgs bosons, gauge bosons and t quark, were computed analytically by following the decay chain down to the production of a b quark, c quark or a tau lepton; the result of the Monte Carlo was used to obtain the final neutrino output. Because of the high column density of the solar medium, the absorption and the energy loss of the produced neutrinos were also included.

One possible effect that we have not included is that of matter-enhanced neutrino oscillations. As pointed out in Ref. [44], these could be important for neutrinos produced by neutralino annihilations in the Sun, if there is a large mixing angle as in some fits to solar or atmospheric neutrino data. It would have been more conservative to allow for $\nu_\mu \rightarrow \nu_e$ or ν_τ oscillations inside the Sun, but we neglect them here.

D. Fluxes of up-going muons

The capability of a neutrino telescope to measure the flux of Eq.(11) depends on how well this signal may be discriminated from the background due to neutrinos produced in the Earth's atmosphere by cosmic rays. In the case of the Sun, the signal to background (S/B)

discrimination is based on the correlation with the position of the Sun in the sky. As far as the signal from the Earth is concerned, the S/B discrimination requires an analysis of the angular distribution, and is based on the property that, whereas the angular distribution of the signal is expected to be markedly peaked at the nadir, the background distribution is almost flat (with a slight increase at the horizon). In order to evaluate these angular distributions properly, one has to take into account the size of the region around the center of the Earth where neutralinos are expected to accumulate, and the physical processes that entail an angular spreading of the signal. Some angular spreading is induced by the $\nu_\mu \rightarrow \mu$ conversion: $\theta_{\mu,\nu} \simeq 2^\circ (E_\nu/100 \text{ GeV})^{-1/2}$, and a comparable effect occurs because of the multiple scattering of the muon in the rock surrounding the detector. Thus, an accurate calculation of angular distributions requires a Monte Carlo simulation [6].

In this paper, since we only deal with spectra, and not with angular distributions, we perform the calculation of the up-going muon fluxes in a simple no-straggling approximation [45]. In fact, this approximation reproduces accurately the Monte Carlo calculations for the distributions in the muon energy [6]. Then, we can write the muon spectrum as [45]

$$\frac{dN_\mu}{dE_\mu} = N_A \frac{1}{A + BE_\mu} \int_{E_{\mu,th}}^{\infty} dE_\nu \frac{dN_\nu}{dE_\nu} \int_{E_\mu}^{E_\nu} dE'_\mu \frac{d\sigma(E_\nu, E'_\mu)}{dE'_\mu} \quad (12)$$

where $E_{\mu,th}$ is the muon energy threshold, N_A is the Avogadro number, $d\sigma(E_\nu, E'_\mu)/dE'_\mu$ is the differential cross section for the production of a μ from a ν_μ impinging on an isoscalar target and $A + BE_\mu$ is the average muon energy loss, due to ionization, pair production, bremsstrahlung and photonuclear effects. For the coefficients A and B we have used the following values $A = 2.4 \cdot 10^{-3} \text{ GeV}/(\text{g}/\text{cm}^2)$, $B = 4.75 \cdot 10^{-6} (\text{g}/\text{cm}^2)^{-1}$ [46].

Let us conclude this section with some comments on the typical parameters of the required experimental layout. In deep underwater/ice experiments muons from neutralino annihilation are planned to be detected using their direct Cerenkov radiation. A relativistic muon in water emits per 1 cm about 250 Cerenkov photons with wavelengths in the interval 300 – 500 nm. Then it is easy to estimate the number of photoelectrons produced in a photomultiplier (PM) at a distance r from muon trajectory as

$$N_e \simeq 30 \frac{Q}{r} D_{PM}^2 \quad (13)$$

where $Q \simeq 0.15 - 0.25$ is the PM quantum efficiency, all distances are given in cm and we take $D_{PM} \simeq 35$ cm as the PM diameter. One can see from Eq.(13) that at a distance equal to the scattering length in the water/ice, which we take as $l_{sc} \sim 20 - 30$ m, PM's detect a strong signal corresponding to about 3 photoelectrons. To determine the muon trajectory, only the PM's located closer than the scattering length can be used. Their number, $N_{PM} \simeq l_\mu l_{sc}^2/d^3$, is of order $100(E_\mu/(100 \text{ GeV}))$ for a distance between detectors $d = 10$ m and a scattering length 25 m.

The supersymmetric model we are discussing is characterized by light neutralinos, $m_\chi \lesssim 200 \text{ GeV}$. This results in a small pathlength of the produced muons, $l_\mu = 500(E_\mu/(100 \text{ GeV}))$ m, which has the following observational consequences.

- For a widely-discussed 1 Km^3 array, many muons have trajectories confined within the detector. The energies of these muons can be estimated from the trajectory lengths.

- There is a small probability to find a big shower due to bremsstrahlung or pair production along the muon trajectory.
- A reliable measurement of the muon trajectory, which is necessary for identification of a neutralino-produced muon, needs a rather dense array with a distance between detectors $d \sim 10$ m in the case of a scattering length 25 - 30 m. It could be the core of a larger detector.

VI. RESULTS AND CONCLUSIONS

In this section we show our results for integrated fluxes Φ_μ of the up-going muons, and compare them with the upper bounds obtained at the present neutrino telescopes. We will then compare these indirect signals with the signals measurable by direct searches for relic neutralinos. We also show how the strengths of the various signals correlate with each other and with the values of the neutralino relic abundance. However, we wish first to comment on some general properties which later provide a simple interpretation of some characteristic features of our numerical results.

(i) Both the event rate for neutralino direct detection R and the capture rate C of a relic neutralino by a celestial body are proportional to $\rho_\chi \sigma_i$. This property also applies to Φ_μ , with some further more complicated dependence on σ_i and σ_{ann} for the flux Φ_μ from the Earth, when equilibrium is not yet established (see Sect. 5.B). Thus, we expect R and Φ_μ to show some similarities in their behaviours as functions of the supersymmetric parameters, when the same elastic cross sections σ_i 's are involved. This is roughly the case, when we consider the indirect signal from the Earth. In fact, in this instance the neutralino capture from the macroscopic body occurs dominantly (except for extremely pure gaugino compositions of the neutralino) through coherent cross sections, which have an overwhelming role also in direct detection by the nuclei considered here. Obviously, this is a qualitative argument, since the difference in the nuclear compositions of the detectors and of the Earth play an important role in the actual numerical results. Furthermore, the similarity between R and Φ_μ^{Earth} is attenuated when equilibrium in the Earth is not yet established, as previously mentioned. A correlation between R and Φ_μ^{Earth} is manifest in some of the figures that will be presented below. At variance with the case of the Earth, it has to be noted that, in some regions of the supersymmetric parameter space, neutralino capture by the Sun occurs mainly through spin-dependent cross sections, due to the overwhelming presence of Hydrogen in the Sun. Under these circumstances, R and the signal from the Sun Φ_μ^{Sun} are not expected necessarily to resemble each other. However, signals which are not enhanced by coherent effects, are generally much below the experimental sensitivities. Summarizing, it is worth remarking that, in view of the previous arguments, direct detection and indirect detection by up-going muons have some common regions of the parameter space to explore, but may also have very distinctive features in their discovery potentials [47].

(ii) If we combine the properties: $R \propto \rho_l \sigma_i$, $\Phi_\mu \propto \rho_l \sigma_i$, and $\Omega_\chi h^2 \propto \sigma_{\text{ann}} v >_{\text{int}}^{-1}$, and take into account the fact that usually σ_i and σ_{ann} , as functions of the supersymmetric model parameters, are either both increasing or both decreasing, we come to the conclusion that the quantities Φ_μ and R are somewhat anticorrelated with $\Omega_\chi h^2$ (see also [48]). This property

is attenuated, but usually not washed out, in the case of scaling of the neutralino local density. In fact, when scaling occurs (*i.e.*, when $\Omega_\chi h^2 < (\Omega h^2)_{\min}$), one has $R \propto \rho_l \xi \sigma_i \propto \rho_l \sigma_i \times [\langle \sigma_{\text{ann}} v \rangle_{\text{int}}]^{-1}$, and the same for Φ_μ . Since it turns out that when σ_i is large also σ_{ann} increases, but in such a way that usually the ratio $\sigma_i/\sigma_{\text{ann}}$ increases too, one can conclude that a form of anticorrelation between $\Omega_\chi h^2$ and Φ_μ (or R) persists also when scaling of ρ_l is effective. A feature of this type is displayed by our numerical results.

Let us turn now to a presentation of some of our results. We show in Fig. 6 a sample of our calculations for the signals expected from the Earth at the representative point $\tan\beta = 53$, for three different choices of the δ_i parameters. The three closed curves denote the boundaries of the allowed regions when the parameters m_0 and $m_{1/2}$ are varied in the ranges $10 \text{ GeV} \leq m_0 \leq 2 \text{ TeV}$, $45 \text{ GeV} \leq m_{1/2} \leq 500 \text{ GeV}$. The figure displays the flux of up-going muons integrated over a cone of half aperture of 30° centered at the nadir, and for muon energies above 1 GeV. Also shown in Fig. 6 is the most stringent experimental bound: $\Phi_\mu^{\text{Earth}} \leq 2.1 \cdot 10^{-14} \text{ cm}^{-2} \cdot \text{s}^{-1}$ (90% C.L.), obtained with an exposure of $2954 \text{ m}^2 \cdot \text{yr}$ [15] (for other recent experimental data see [49–51]).

In Fig. 6(a) we notice, in the case $\delta_1 = 0$, $\delta_2 = 0$, $\alpha_s = 0.1127$ indicated by the solid line, a decreasing behaviour of Φ_μ as a function of the neutralino mass, as expected from the structure of the capture rate C . It is remarkable that for some neutralino configurations in the interesting range $m_\chi \simeq 150 \text{ GeV}$ the present experimental sensitivity (or a slight improvement of it) is already adequate for restricting the supersymmetric parameter space. These configurations have a light A : $M_A \lesssim 70 \text{ GeV}$. The correlations between Φ_μ and $\Omega_\chi h^2$ or between Φ_μ and R , anticipated in points (i) and (ii) above, are apparent in parts (b) and (c) of Fig. 6, respectively. One important feature of this parameter choice is shown by the solid line in Fig. 6(b): the neutralino configurations, which are explorable with measurements of Φ_μ , yield values of $\Omega_\chi h^2$ below the range of Eq.(4). We stress that this is a general trend, which will be further discussed at the end of this Section. Fig. 6(c) shows how measurements of Φ_μ and R may give information about similar neutralino configurations. The event rate for direct detection R , employed in the present paper as well as in our previous work [14], is defined as the integral of dR/dE_{ee} (E_{ee} is the electron equivalent energy) over the 12-13 KeV range, for a Ge detector. The experimental upper bound is that obtained from the experiment of Ref. [52] (for other experiments using Ge detectors see Ref. [53]).

The discovery potential of neutrino telescopes in this context is further illustrated in Fig.7, where the case denoted by the solid line in Fig 6 is shown. This figure displays (by empty squares) the region in the $m_{1/2} - m_0$ plot (and in the $m_{1/2} - \mu$ plot) which may be explored by a neutrino telescope whose sensitivity is one order of magnitude better than that of Ref. [15]. The region denoted by light crosses would require an even better sensitivity. In this connection, we stress that the theoretical results presented here were obtained using a particular set of representative values, not only for some supersymmetric model parameters, but also for a number of astrophysical and cosmological parameters, many of which are affected by large experimental uncertainties. This is the case, for instance, of the dark matter local density ρ_l and of Ωh^2 . For this reason, one has to be extremely cautious in extracting exclusion plots in the supersymmetric parameters from a comparison between present experimental and theoretical values of Φ_μ . Obviously, a region of the neutralino parameter space would be excluded only if the theoretical values, obtained with *the most conservative set of values for the free parameters*, were above the experimental upper bound.

This is certainly not the case with the present experimental limits. Particular attention has to be paid to the value of the neutralino local density ρ_χ to be used. Just employing $\rho_\chi = \rho_l$ everywhere, without making a consistency check with the value of $\Omega_\chi h^2$ and without rescaling appropriately, leads to erroneous exclusion plots.

In Fig.6 we present as dashed lines another set of results, corresponding to a case where a departure from universality in soft scalar masses is introduced: $\delta_1 = 0, \delta_2 = -0.3$. We notice that many configurations may produce signals above the experimental bounds, both in direct and indirect searches. The dashed lines exhibit correlations between the various quantities similar to those exhibited by the solid lines, although in this case some configurations provide both a measurable Φ_μ and an $\Omega_\chi h^2$ in the range of Eq. (4). The configurations whose signals are above the experimental limit are displayed in Fig. 8 with heavy oblique crosses. In particular, from Fig. 8(b) it is clear that the corresponding neutralino compositions are dominantly gaugino-like (notice that the allowed region in the $m_{1/2}-\mu$ plane extends to the right of the line $m_0 = m_{0,min}$, due to a negative value of the coefficient J_2 of Eq.(6)). It is worth recalling that the strict $m_{1/2}-\mu$ correlation appearing in Fig. 7 is removed here, due to the deviation from universality we have introduced (the coefficient J_2 is positive and sizeable here). The reason why many configurations are above the experimental bound, in spite of their gaugino nature, is the fact that in these configurations the CP-odd Higgs neutral boson A is light: $m_A \lesssim 65$ GeV (the coefficient K_2 of Eq.(7) is negative).

One further example of a non-universal case is provided by the dotted lines in Fig. 6 and by Fig. 9, where $\delta_1 = 0.7, \delta_2 = 0.4$. A number of configurations turn out again to exceed the experimental bound. Here the neutralino parameter space opens up to the left of the line $m_0 = m_{0,min}$, where gaugino-higgsino mixture takes place. Again, the configurations with the highest signals have a light A boson.

Examples of signals from the Sun, Φ_μ^{Sun} , are shown in Figs. 10 and 11 together with the value of the experimental bound: $\Phi_\mu^{Sun} \leq 3.5 \cdot 10^{-14} \text{ cm}^{-2} \cdot \text{s}^{-1}$ (90% C.L.), obtained with an exposure of $1002 \text{ m}^2 \cdot \text{yr}$ [15]. By comparing with Fig. 6, we notice that the distribution of points along the vertical axis is much more spread out in the case of the signal from the Earth than from the Sun, with many configurations giving values of Φ_μ^{Earth} far below (by many orders of magnitude) the experimental sensitivity. The strong attenuation of Φ_μ^{Earth} for these configurations is due to the fact that for them the capture-annihilation equilibrium in the Earth is far from being established. As for the signals from the Sun, we further note that for all configurations of Fig. 10 the signal is dominated by coherent contributions, in spite of the scarcity of heavy nuclei in the Sun. This makes the discovery potential for the signal from the Sun essentially equivalent to the one for the signal from the Earth, at this representative point. Spin-dependent effects contribute only for a few per cent, at most. In other representative points, the main contribution to the signal may be due to non-coherent cross sections. However, under these circumstances the overall signal is much smaller than the experimental limit.

In all the examples just discussed (Figs. 6–11), referring to the representative value $\tan\beta = 53$, we have found that measurements of Φ_μ provides a useful tool for investigating interesting regions of the supersymmetric parameter space, when the boson A is light, $M_A = O(M_Z)$. Unfortunately, but unavoidably, the very fact that M_A is small makes it difficult for these supersymmetric configurations to yield a neutralino relic density in the desired range:

$0.1 \lesssim \Omega_\chi h^2 \lesssim 0.3$. A quite opposite scenario occurs in different, and equally allowed, sectors of the parameter space, such as those examined in Sect.4, where $\Omega_\chi h^2$ is very large (and where the signals R and Φ_μ are much below the present and the foreseeable experimental sensitivities). This is typically a scenario of small $\tan\beta$ or it may occur at large $\tan\beta$ with deviations from m_0 universality (see, for instance, the case illustrated in Fig. 3). It is remarkable that both scenarios are possible in the case of the supergravity–inspired model adopted in the present paper, although it is constrained by the requirement of radiative EWSB. Of course, much wider regions of the parameter space are allowed to both scenarios in the case of the unconstrained MSSM.

Acknowledgements.

This work was supported, in part, by the Human Capital and Mobility Programme of the European Economic Community under contract No. CHRX-CT93-0120 (DG 12 COMA) and by the Research Funds of the Ministero dell’Università e della Ricerca Scientifica e Tecnologica. Also a fellowship of the Istituto Nazionale di Fisica Nucleare is gratefully acknowledged by N. Fornengo and one of the Università di Torino by G. Mignola.

REFERENCES

- [1] J. Ellis, J. S. Hagelin, D. V. Nanopoulos, K. Olive and M. Srednicki, *Nucl. Phys.* **B238** (1984) 453.
- [2] M. White, D. Scott and J. Silk, *Ann. Rev. Astron. Astrophys.* **32** (1994) 319;
M. White and D. Scott, astro-ph/9601170.
- [3] For reviews on detection methods for dark matter candidates, see J. R. Primack, D. Seckel and B. Sadoulet, *Ann. Rev. Nucl. Part. Sci.* **38** (1988) 751, and P. F. Smith and J. D. Lewin, *Phys. Rep.* **187** (1990) 203. An up-dated review of the phenomenology of neutralino dark matter is presented in G. Jungman, M. Kamionkowski and K. Griest, Syracuse University preprint SU-4240-505, (1995).
- [4] See, for instance, R. Bernabei, *Riv. N. Cim.* **18** (1995) N.5, and L. Mosca, invited talk at TAUP 95 (Toledo, September 1995) to appear in *Nucl. Phys. B* (Proc. Suppl.).
- [5] G.F. Giudice and E. Roulet, *Nucl. Phys.* **B316** (1989) 429;
G.B. Gelmini, P. Gondolo and E. Roulet, *Nucl. Phys.* **B351** (1991) 623;
M. Kamionkowski, *Phys. Rev.* **D44** (1991) 3021;
A. Bottino, V. de Alfaro, N. Fornengo, G. Mignola and M. Pignone, *Phys. Lett.* **B265** (1991) 57;
F. Halzen, M. Kamionkowski and T. Steltzer, *Phys. Rev.* **D45** (1992) 4439;
V.S. Berezinsky, *Nucl. Phys.* (Proc. Suppl.) **B31** (1993) 413 (Proc. Neutrino 92, Ed. A. Morales)
M. Mori et al., *Phys. Rev.* **D48** (1993) 5505;
M. Drees, G. Jungman, M. Kamionkowski and M.M. Nojiri, *Phys. Rev.* **D49** (1994) 636;
R. Gandhi, J.L. Lopez, D.V. Nanopoulos, K. Yuan and A. Zichichi, *Phys. Rev.* **D49** (1994) 3691.
- [6] A. Bottino, N. Fornengo, G. Mignola and L. Moscoso, *Astroparticle Physics* **3** (1995) 65.
- [7] For a review of the new experimental projects of neutrino telescopes, see L. Resvanis, invited talk at TAUP 95 (Toledo, September 1995) to appear in *Nucl. Phys. B* (Proc. Suppl.).
- [8] J. Ellis, S. Kelley and D. Nanopoulos, *Phys. Lett.* **B260** (1991) 131;
U. Amaldi, W. de Boer and H. Fürstenau, *Phys. Lett.* **B260** (1991) 447;
P. Langacker and M. Luo, *Phys. Rev.* **D44** (1991) 817.
- [9] J. Ellis, G. L. Fogli and E. Lisi, CERN preprint TH/95-202 (1995) and references therein.
- [10] H. P. Nilles, *Phys. Rep.* **110** (1984) 1;
H. E. Haber and G. L. Kane, *Phys. Rep.* **117** (1985) 75;
R. Barbieri *Riv. Nuovo Cim.* **11** (1988) 1.
- [11] L. E. Ibañez and C. Lopez, *Nucl. Phys.* **B233** (1984) 511;
J. Ellis and F. Zwirner, *Nucl. Phys.* **B338** (1990) 317;
J. Ellis and L. Roszkowski, *Phys. Lett.* **B283** (1992) 252;
M. Drees and M. M. Nojiri, *Nucl. Phys.* **B369** (1992) 54;
M. Olechowski and S. Pokorski, *Nucl. Phys.* **B404** (1993) 590;
R.G. Roberts and L. Roszkowski, *Phys. Lett.* **B309** (1993) 329;

- R. Arnowitt and P. Nath, Brazil Summer School **3** (1993) 63 (hep-ph/9309277);
 J. L. Lopez, D.V. Nanopoulos and A. Zichichi, *Riv. Nuovo Cim.* **17** (1994) 1;
 W. de Boer, R. Ehret and D.I. Kazakov, Karlsruhe University preprint IEKP-KA/94-04 (1994);
 G. L. Kane, C. Kolda, L. Roszkowski and J. D. Wells, *Phys. Rev.* **D49** (1994) 6173;
 P. Nath and R. Arnowitt, *Phys. Rev. Lett.* **74** (1995) 4592;
 X. Wang, J. Lopez and D. Nanopoulos, *Phys. Lett.* **B348** (1995) 105;
 R. Rattazzi and U. Sarid, *Phys. Rev.* **D53** (1996) 1553.
- [12] M. Olechowski and S. Pokorski, *Phys. Lett.* **B344** (1995) 201.
- [13] N. Polonsky and A. Pomarol, *Phys. Rev. Lett.* **73** (1994) 2292; *Phys. Rev.* **D51** (1995) 6532;
 D. Matalliotakis and H. P. Nilles, *Nucl. Phys.* **B435** (1995) 115;
 A. Pomarol and S. Dimopoulos, CERN preprint CERN-TH/95-114 (1995);
 H. Murayama, Berkeley preprint LBL-36962 (1995).
- [14] V. Berezhinsky, A. Bottino, J. Ellis, N. Fornengo, G. Mignola and S. Scopel, preprint CERN-TH 95-206 (to appear in *Astroparticle Physics*).
- [15] M.M. Boliev et al. (Baksan Telescope), contribution presented by S.P. Mikheyev at TAUP 95 (Toledo, September 1995) to appear in *Nucl. Phys. B* (Proc. Suppl.) and S.P. Mikheyev, private communication.
- [16] M. Rowan-Robinson, Les Houches lectures (1993) and CERN Colloquium (1995).
- [17] W. L. Freedman et al., *Nature* **371** (1994) 757.
- [18] N. R. Tanvir, T. Shanks, H. C. Ferguson and D. R. T. Robinson, *Nature* **377** (1995) 399.
- [19] K. Fisher et al., Princeton preprint IASSNS-AST-95-19 (1995);
 S. Zaroubi, A. Dekel, Y. Hoffman and T. Kolatt, astro-ph/9603068.
- [20] A. Dekel, *Ann. Rev. of Astron. and Astrophys.* **32** (1994) 371.
- [21] N. Hata, R. J. Scherrer, G. Steigman, D. Thomas and T. P. Walker Preprint OSU-TA 26/94 (1994), submitted to *Ap. J. Lett.*;
 C. J. Copi, D. N. Schramm and M. S. Turner, *Science* **267** (1995) 192 and *Phys. Rev. Lett.* **75** (1995) 3981;
 S. Sarkar, Oxford University preprint OUTP-95-16-P (1995);
 B. D. Fields, K. Kainulainen, K. A. Olive and D. Thomas, CERN preprint CERN-TH-96-59 (1996).
- [22] C. L. Bennett et al., COBE preprint 96-01 astro-ph/9601067.
- [23] M. J. Geller, J. P. Huchra, *Ap. J. Suppl.* **52** (1983) 61.
- [24] A. Klypin, S. Borgani, J. Holtzman and J. R. Primack, *Ap. J.* **444** (1995) 1.
- [25] J. R. Primack, J. Holtzman, A. Klypin and D. O. Caldwell, *Nucl. Phys. B* (Proc. Suppl.) **43** (1995) 133.
- [26] J. R. Primack, to be published in Proc. of 1994 DPF Summer Study on High Energy Physics: Particle and Nuclear Astrophysics and Cosmology in the Next Millennium (Snowmass 94).
- [27] C. J. Copi and D. N. Schramm, astro-ph/9504026.
- [28] L. Rolandi, H. Dijkstra, D. Strickland and G. Wilson, representing the ALEPH, DELPHI, L3 AND OPAL collaborations, Joint Seminar on the First Results from LEP 1.5, CERN, December 1995.

- [29] J. Ellis, K. Enqvist, D. V. Nanopoulos and F. Zwirner, *Mod. Phys. Lett.* **A1** (1986) 57;
R. Barbieri and G. Giudice, *Nucl. Phys.* **B306** (1988) 63;
M. Olechowski and S. Pokorski, *Nucl. Phys.* **B404** (1993) 590;
B. de Carlos and J. A. Casas, *Phys. Lett.* **B309** (1993) 320.
- [30] V. Barger, M. S. Berger and P. Ohmann, *Phys. Rev.* **D49** (1994) 4908;
G. W. Anderson and D. J. Castaño, *Phys. Rev.* **D52** (1995) 1693;
S. Dimopoulos and G. Giudice, CERN preprint TH/95-188 (1995).
- [31] P.H. Chankowski and S. Pokorski, preprint MPI-PhT/95-49 (hep-ph 9505308);
D. Garcia and J. Solà, *Phys. Lett.* **B354** (1995) 335;
G.L. Kane, R.G. Stuart and J.D. Wells, *Phys. Lett.* **B354** (1995) 350.
- [32] M. Srednicki, R. Watkins and K. Olive, *Nucl. Phys.* **B310** (1988) 693;
J. Ellis, L. Roszkowski and Z. Lalak, *Phys. Lett.* **B245** (1990) 545.
- [33] G. Gelmini and P. Gondolo, *Nucl. Phys.* **B360** (1991) 145.
- [34] K. Griest, M. Kamionkowski and M. S. Turner, *Phys. Rev.* **D41** (1990) 3565;
M. Drees and M. M. Nojiri, *Phys. Rev.* **D47** (1993) 3776.
- [35] A. Bottino, V. de Alfaro, N. Fornengo, G. Mignola and M. Pignone, *Astroparticle Physics* **2** (1994) 67.
- [36] E. I. Gates, G. Gyuk and M. S. Turner, FNAL preprint FERMILAB-PUB-95/090-A, (1995).
- [37] R.A. Flores, *Phys. Lett.* **B215** (1988) 73
- [38] A. Gould, *Ap. J.* **321** (1987) 571; *Ap. J.* **328** (1988) 919; *Ap. J.* **368** (1991) 610.
- [39] K. Griest and D. Seckel, *Nucl. Phys.* **B283** (1987) 681.
- [40] M. Drees, G. Jungman, M. Kamionkowski and M.M. Nojiri, *Phys. Rev.* **D49** (1994) 636
- [41] J.Edsjö and P. Gondolo, preprint PAR/LPTHE/95-12.
- [42] T. Sjöstrand, *Comp. Phys. Comm.* **39** (1986) 347; *Comp. Phys. Comm.* **43** (1987) 367;
CERN-TH 6488/92.
- [43] S.Ritz and D.Seckel, *Nucl. Phys.* **B304** (1988) 877.
- [44] J. Ellis, R. A. Flores and S. S. Masood, *Phys. Lett* **B294** (1992) 229.
- [45] T.K. Gaisser, *Cosmic Rays and Particle Physics*, Cambridge University Press, 1992.
- [46] A. Bottino, V. de Alfaro, N. Fornengo, G. Mignola and M. Pignone, *Phys. Lett.* **B265** (1991) 57.
- [47] Other indirect signals, due to neutralino annihilation in the halo, may show an even more pronounced difference. See for instance: A. Bottino, C. Favero, N. Fornengo and G. Mignola, *Astroparticle Physics* **3** (1995) 77.
- [48] L. Bergstöm and P. Gondolo, Uppsala University preprint UUITP-17-95 (1995).
- [49] M. Mori et al. (Kamiokande Collaboration), *Phys. Rev.* **48** (1993) 5505.
- [50] M. Ambrosio et al. (MACRO Collaboration), contribution presented by T. Montaruli at TAUP 95 (Toledo, September 1995) to appear in *Nucl. Phys.* **B** (Proc. Suppl.).
- [51] L.B. Bezrukov et al. (Baikal Underwater Telescope), contribution presented by J. Djilkibaev at "The Dark Side of the Universe" (Rome, November 1995) to appear in the Proceedings.
- [52] M. Beck, (Heidelberg-Moscow Collaboration), TAUP93 Proceedings, *Nucl. Phys.* **B** (Proc Suppl) **35** (1994) 150.
- [53] S. P. Ahlen et al., *Phys. Lett.* **B195** (1987) 603;
D. O. Caldwell et al., *Phys. Rev. Lett.* **61** (1988) 510;

A.K. Drukier et al., TAUP91 Proceedings, *Nucl. Phys. B* (Proc. Suppl.) **28A** (1992) 293;
I. R. Sagdev, A. K. Drukier, D. J. Welsh, A. A. Klimenko, S. B. Osetrov, A. A. Smolnikov, TAUP93 proceedings, *Nucl. Phys. B* (Proc. Suppl.) **35** (1994) 175;
M. L. Sarsa et al., *ibidem* 154;
D. Reusser et al., *Phys. Lett.* **B255** (1991) 143.

Figure Captions

Figure 1 – Coefficients J_1, J_2 and K_1, K_2 of the polynomial expressions (6,7) as functions of $\tan \beta$. The range $1.5 \leq \tan \beta \leq 4$ is shown in section (a) and the range $4 \leq \tan \beta \leq 53$ in section (b). In the upper part J_1 is denoted by a solid line, J_2 by a dot–dashed line. In the lower part, K_1 is denoted by a solid line, K_2 by a dot–dashed line.

Figure 2 – a) The parameter space in the $(m_{1/2}, m_0)$ plane for $\tan \beta = 1.5$, $\delta_1 = 0$ and $\delta_2 = 0$, $\alpha_s = 0.1127$. The empty regions are excluded by: i) accelerator constraints, ii) radiative EWSB conditions, iii) the LSP not being a neutralino. Dots represent the region where $\Omega_\chi h^2 > 1$. Regions with crosses are excluded by $b \rightarrow s\gamma$ and m_b constraints. In the regions denoted by filled diamonds, $0.1 \leq \Omega_\chi h^2 \leq 0.3$. b) The parameter space represented in the $(m_{1/2}, \mu)$ plane. The line $m_0 = m_{0,min}$ corresponds to the minimum value of m_0 . Notations are the same as in a), but crosses are omitted here. The dashed lines denote the no–fine–tuning upper bounds on m_0 , $m_{1/2}$ and μ .

Figure 3 – The same as in Figure 2, but with $\delta_1 = -1.0$ and $\delta_2 = 1.0$.

Figure 4 – The same as in Figure 2, but with $\tan \beta = 53$, $\delta_1 = 0.4$ and $\delta_2 = -0.1$. $\alpha_s = 0.1127$.

Figure 5 – The same as in Figure 4, but with $\alpha = 0.118$.

Figure 6 – The flux Φ_μ^{Earth} for $\tan \beta = 53$: $\delta_1 = 0$, $\delta_2 = 0$ and $\alpha_s = 0.1127$ (solid line), $\delta_1 = 0$, $\delta_2 = -0.3$ and $\alpha_s = 0.118$ (dashed line), and $\delta_1 = 0.7$, $\delta_2 = 0.4$ and $\alpha_s = 0.115$ (dotted line) as a function of m_χ (a), as a function of $\Omega_\chi h^2$ (b), and plotted versus the rate for direct detection with a Ge detector (c). Allowed configurations stay inside the closed curves. The horizontal line displays the experimental bound $\Phi_\mu^{Earth} \leq 2.1 \cdot 10^{-14} \text{ cm}^{-2} \cdot \text{s}^{-1}$ (90% C.L.) [15], and the vertical line of section (c) displays the upper limit of Ref. [52]. Parameters are varied on a linear equally–spaced grid over the ranges: $10 \text{ GeV} \leq m_0 \leq 2 \text{ TeV}$, $45 \text{ GeV} \leq m_{1/2} \leq 500 \text{ GeV}$.

Figure 7 – a) The parameter space in the $(m_{1/2}, m_0)$ plane for $\tan \beta = 53$, $\delta_1 = 0$ and $\delta_2 = 0$, $\alpha_s = 0.1127$. Empty regions are excluded by: i) accelerator constraints, ii) radiative EWSB conditions, iii) the LSP not being a neutralino, iv) $b \rightarrow s\gamma$ and m_b constraints. The heavy oblique crosses denote configurations above the present experimental bound [15]. Squares denote regions which could be explored by a neutrino telescope whose sensitivity is

one order of magnitude better than that of Ref. [15]. The region with light crosses would require an even better sensitivity. b) The parameter space represented in the $(m_{1/2}, \mu)$ plane.

Figure 8 – The same as in Figure 7, but with $\delta_1 = 0$ and $\delta_2 = -0.3$, $\alpha_s = 0.118$.

Figure 9 – The same as in Figure 8, but with $\delta_1 = 0.7$ and $\delta_2 = 0.4$, $\alpha_s = 0.115$.

Figure 10 – The flux Φ_μ^{Sun} for $\tan\beta = 53$, $\delta_1 = 0$ and $\delta_2 = -0.3$, $\alpha = 0.118$, as a function of m_χ (a), as a function of $\Omega_\chi h^2$ (b), and plotted versus the rate for direct detection with a Ge detector (c). Allowed configurations stay inside the closed curves. The horizontal line displays the experimental bound $\Phi_\mu^{Sun} \leq 3.5 \cdot 10^{-14} \text{ cm}^{-2} \cdot \text{s}^{-1}$ (90% C.L.) [15], and the vertical line of section (c) displays the upper limit of Ref. [52]. Parameters are varied on a linear equally-spaced grid over the ranges: $10 \text{ GeV} \leq m_0 \leq 2 \text{ TeV}$, $45 \text{ GeV} \leq m_{1/2} \leq 500 \text{ GeV}$.

Figure 11 – a) The parameter space in the $(m_{1/2}, m_0)$ plane for $\tan\beta = 53$, $\delta_1 = 0$ and $\delta_2 = -0.3$, $\alpha_s = 0.118$. Empty regions are excluded by: i) accelerator constraints, ii) radiative EWSB conditions, iii) the LSP not being a neutralino, iv) $b \rightarrow s\gamma$ and m_b constraints. The heavy oblique crosses denote configurations above the present experimental bound: $\Phi_\mu^{Sun} \leq 3.5 \cdot 10^{-14} \text{ cm}^{-2} \cdot \text{s}^{-1}$ (90% C.L.) [15]. Squares denote regions which could be explored by a neutrino telescope whose sensitivity is one order of magnitude better than that of Ref. [15]. The region with light crosses would require an even better sensitivity. b) The parameter space represented in the $(m_{1/2}, \mu)$ plane.

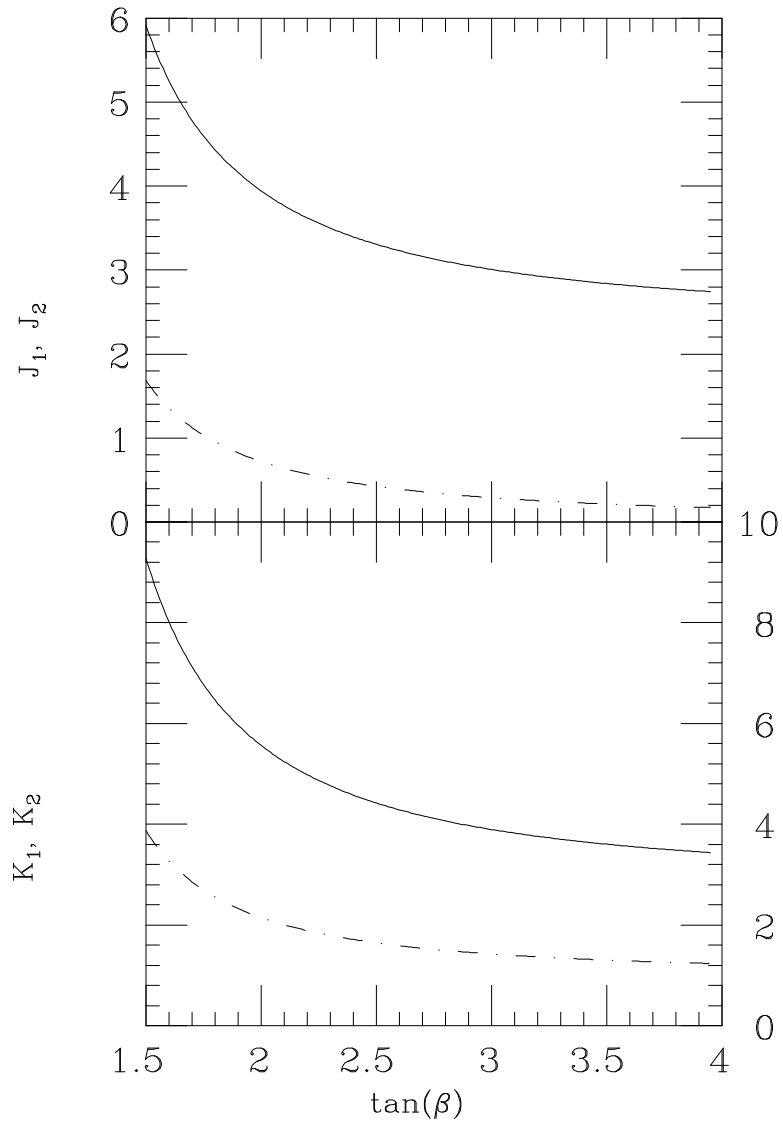


Figure 1a

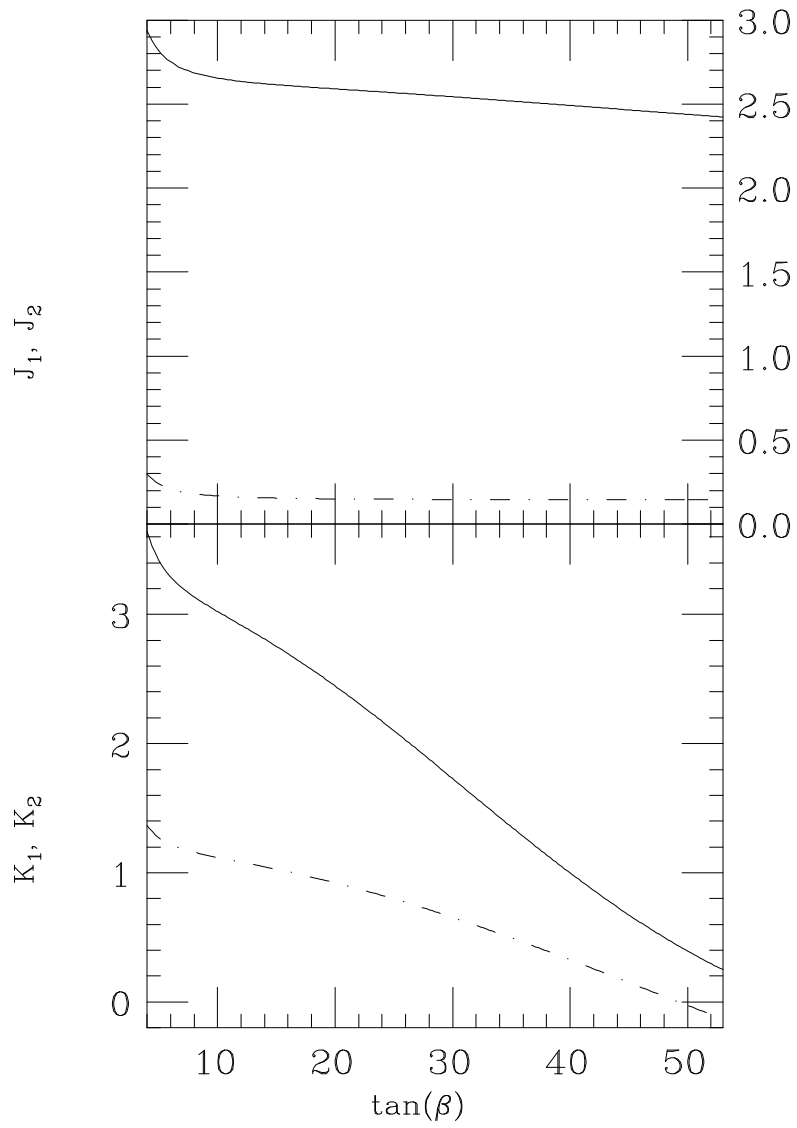


Figure 1b

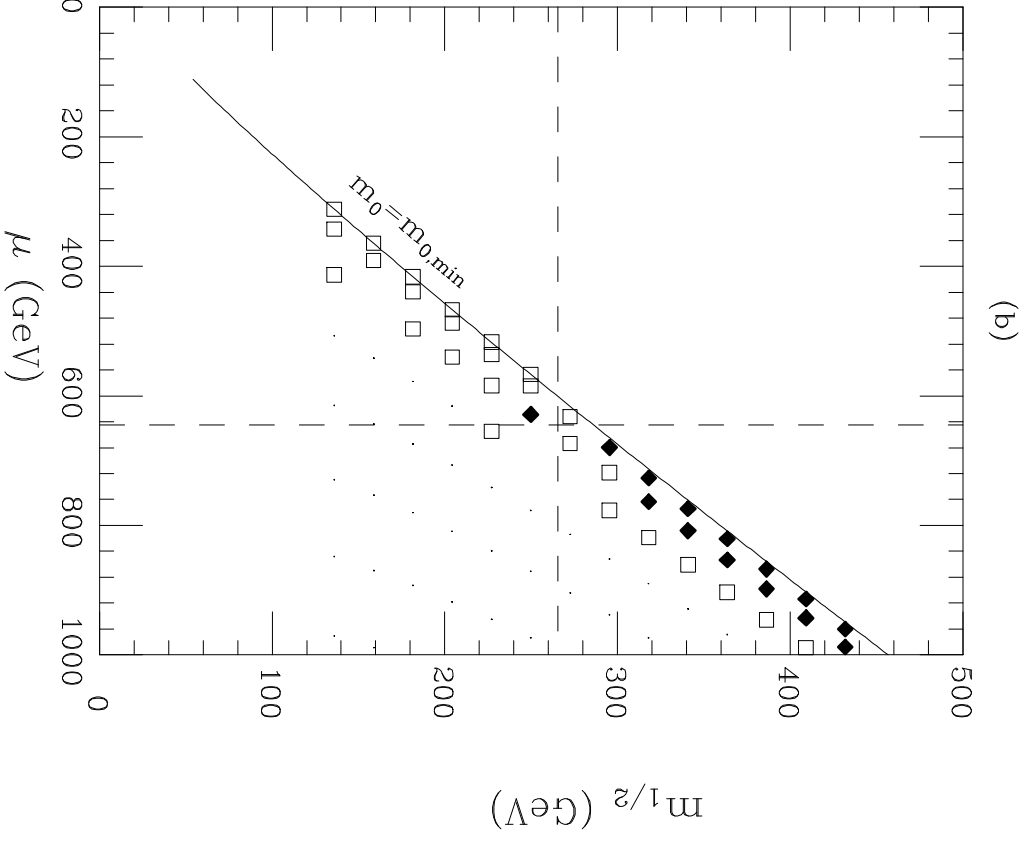
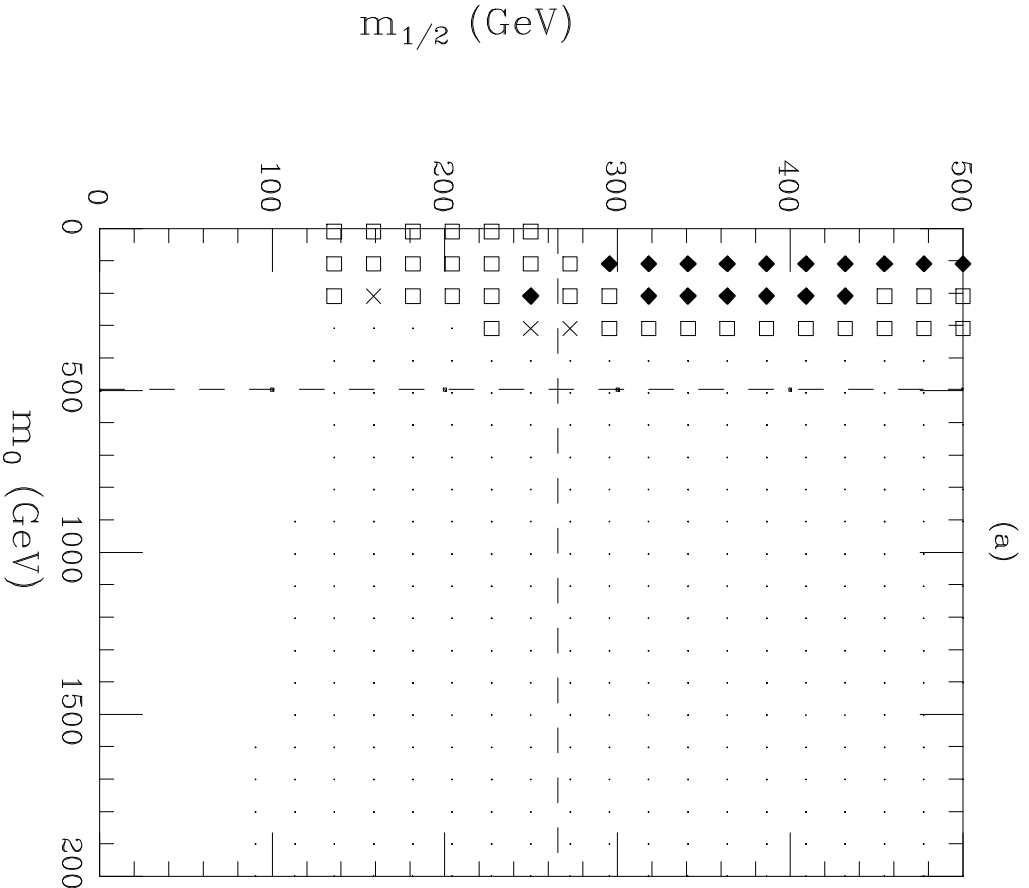


Figure 2

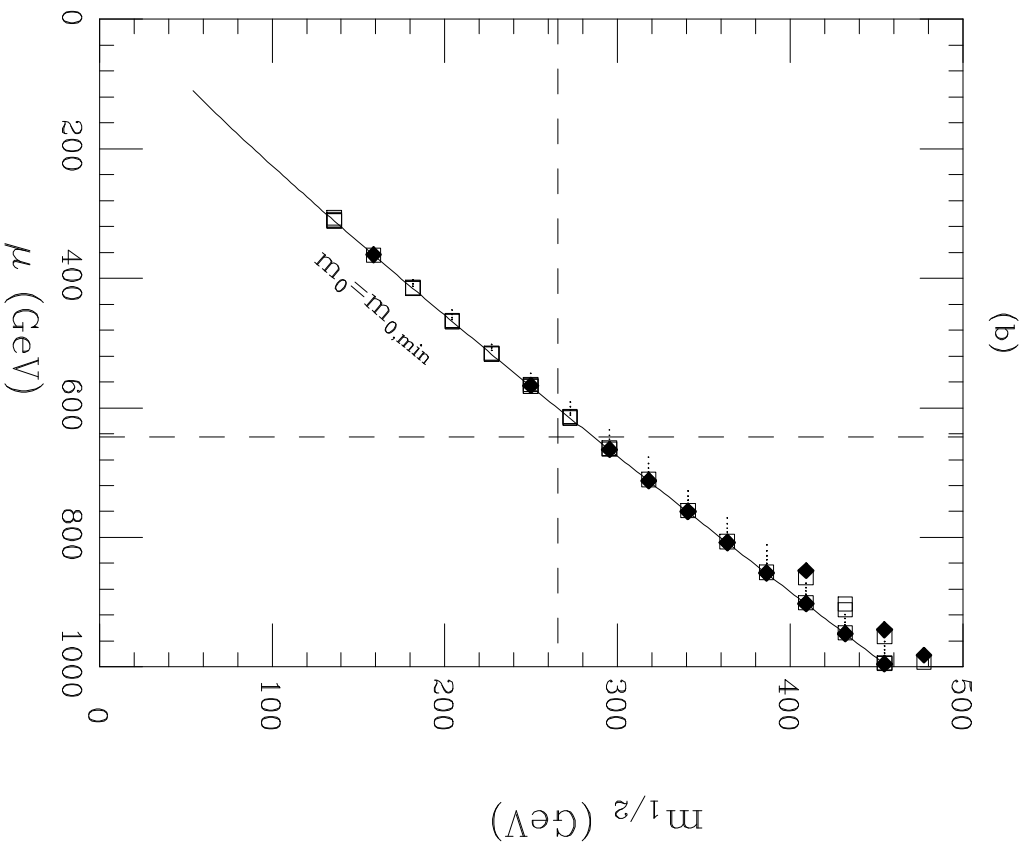
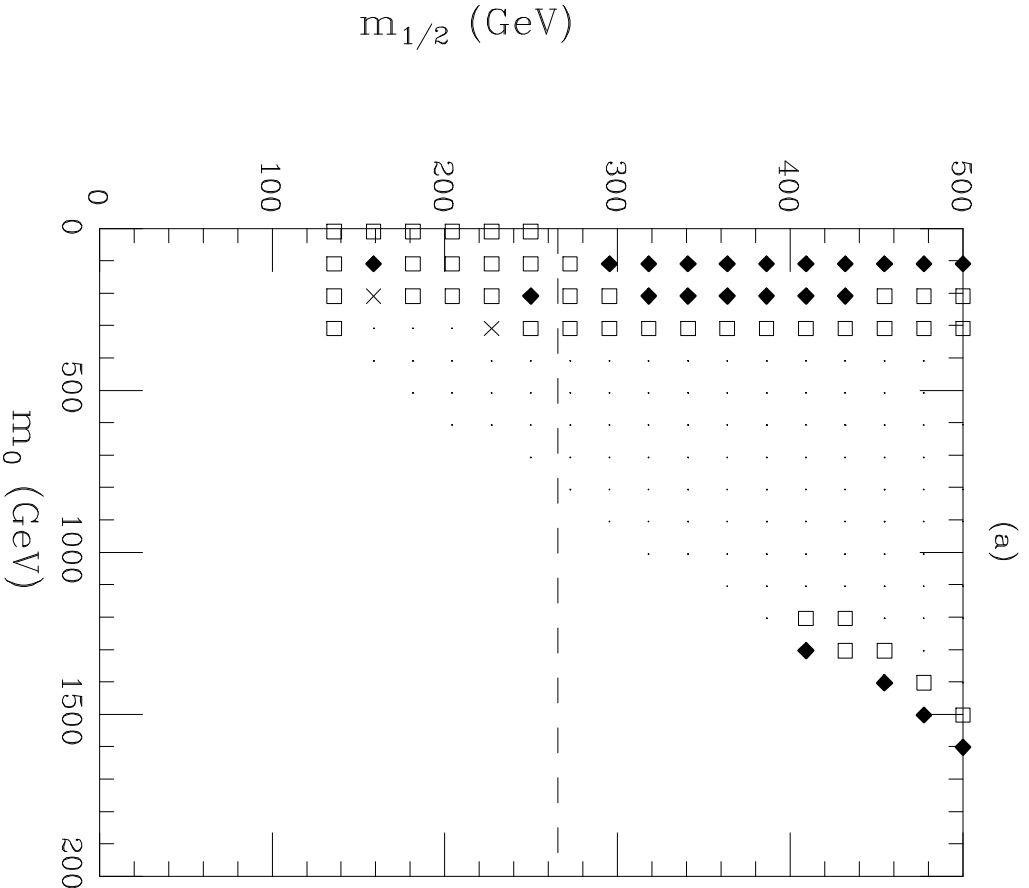


Figure 3

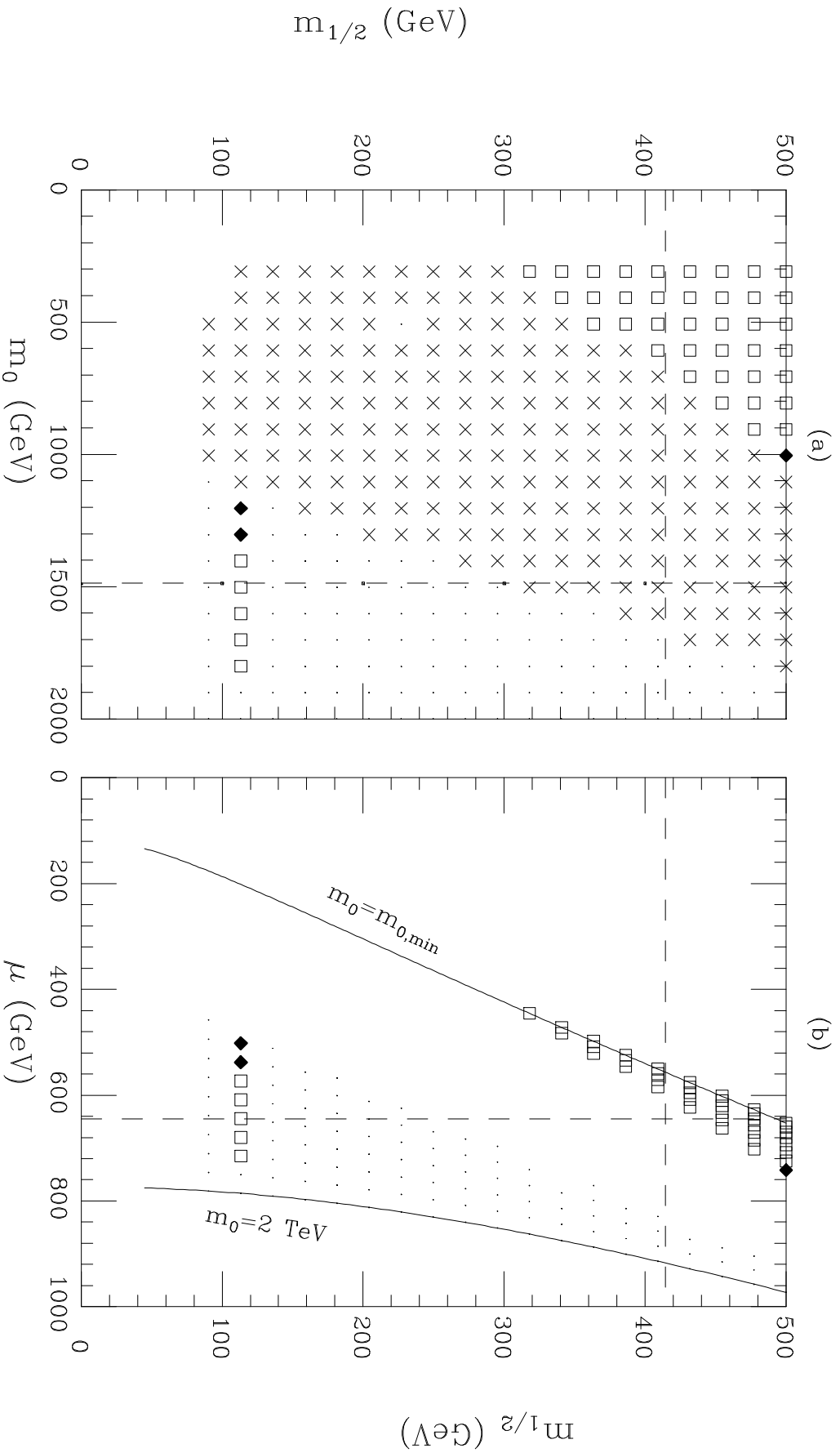


Figure 4

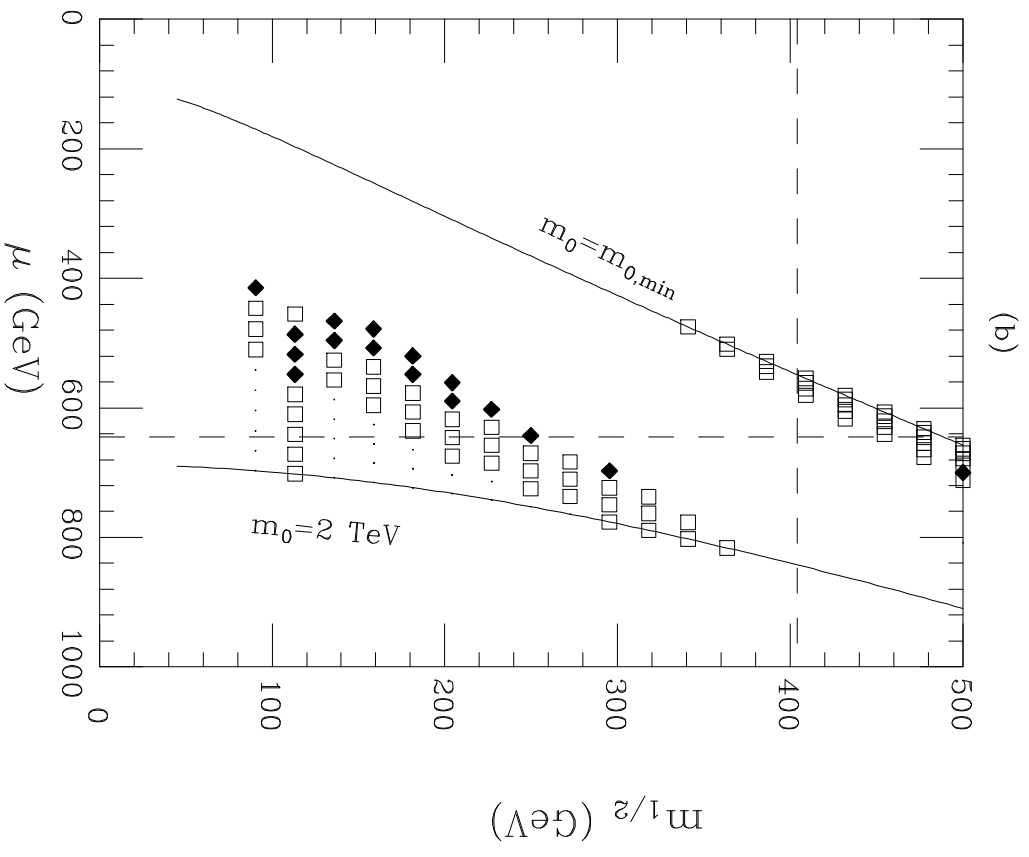
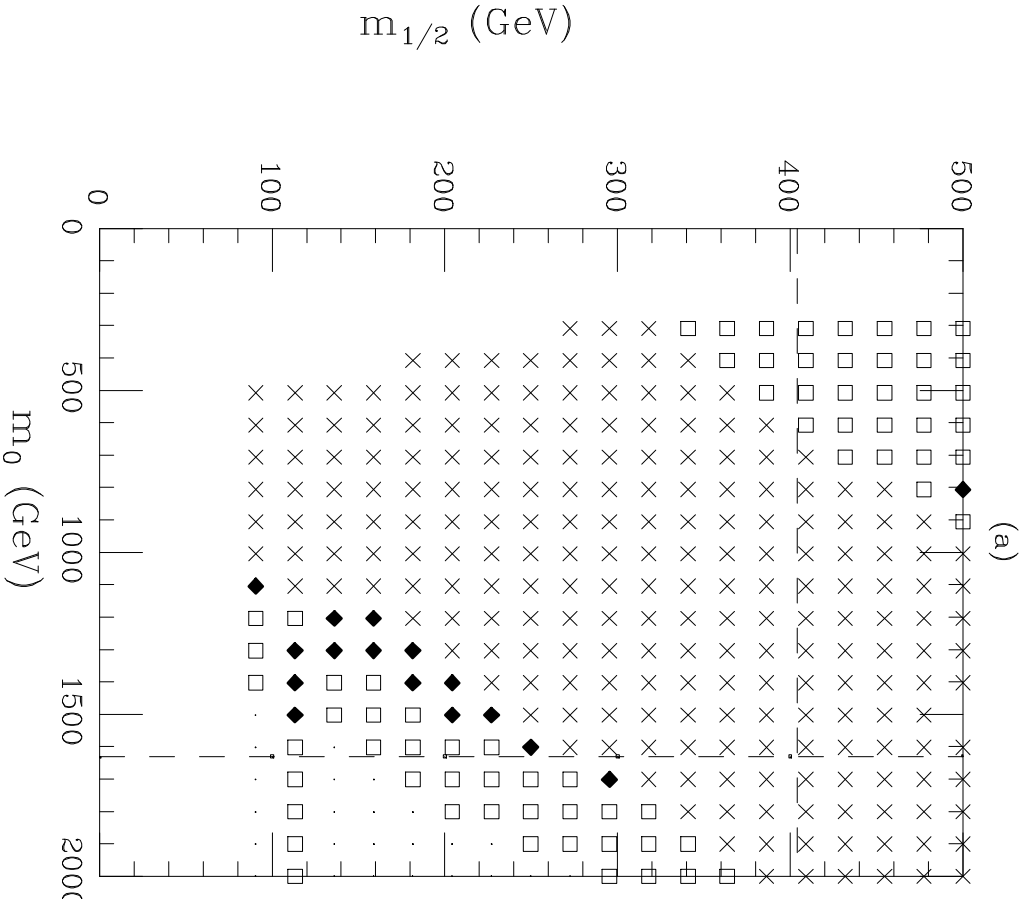


Figure 5

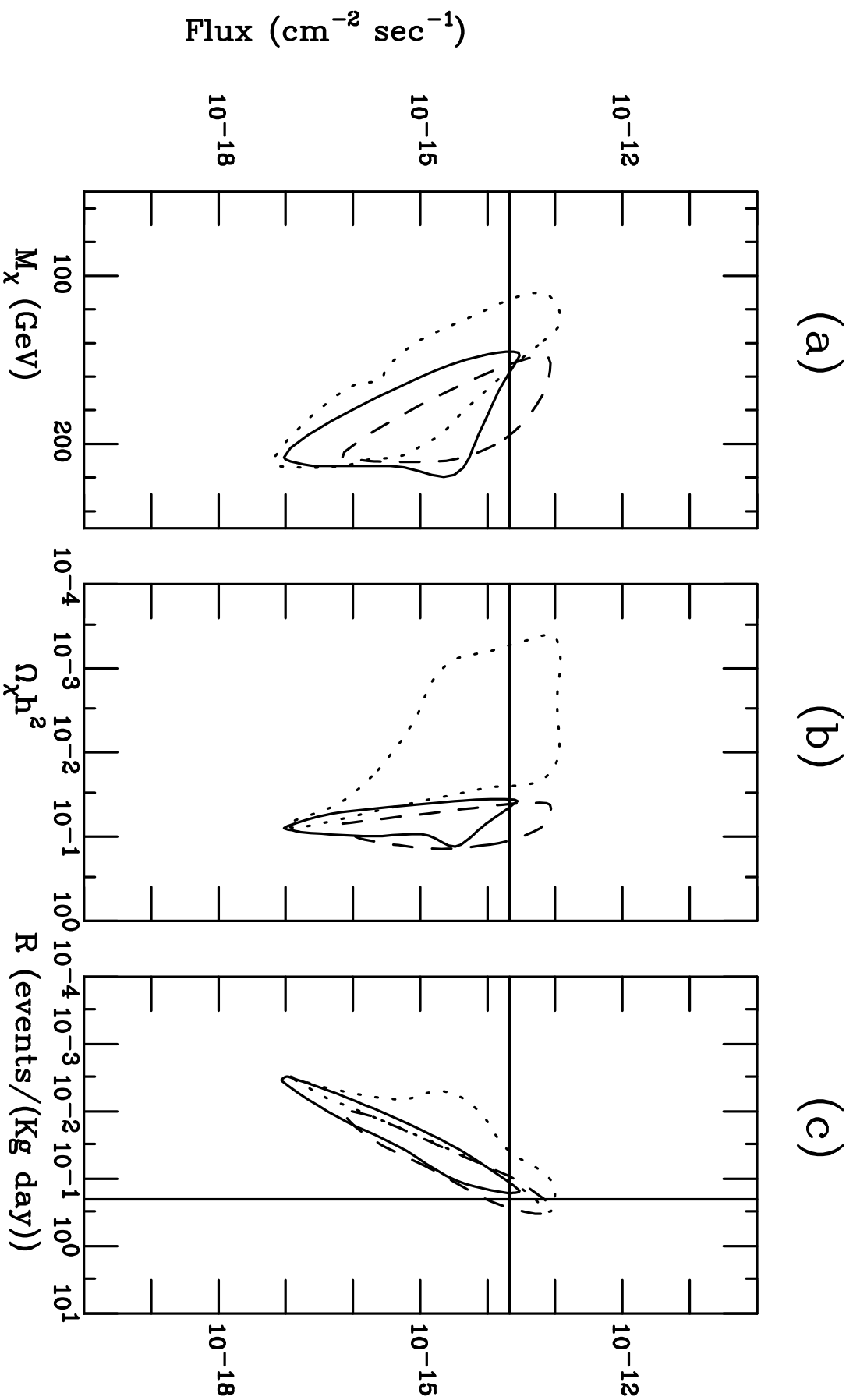


Figure 6

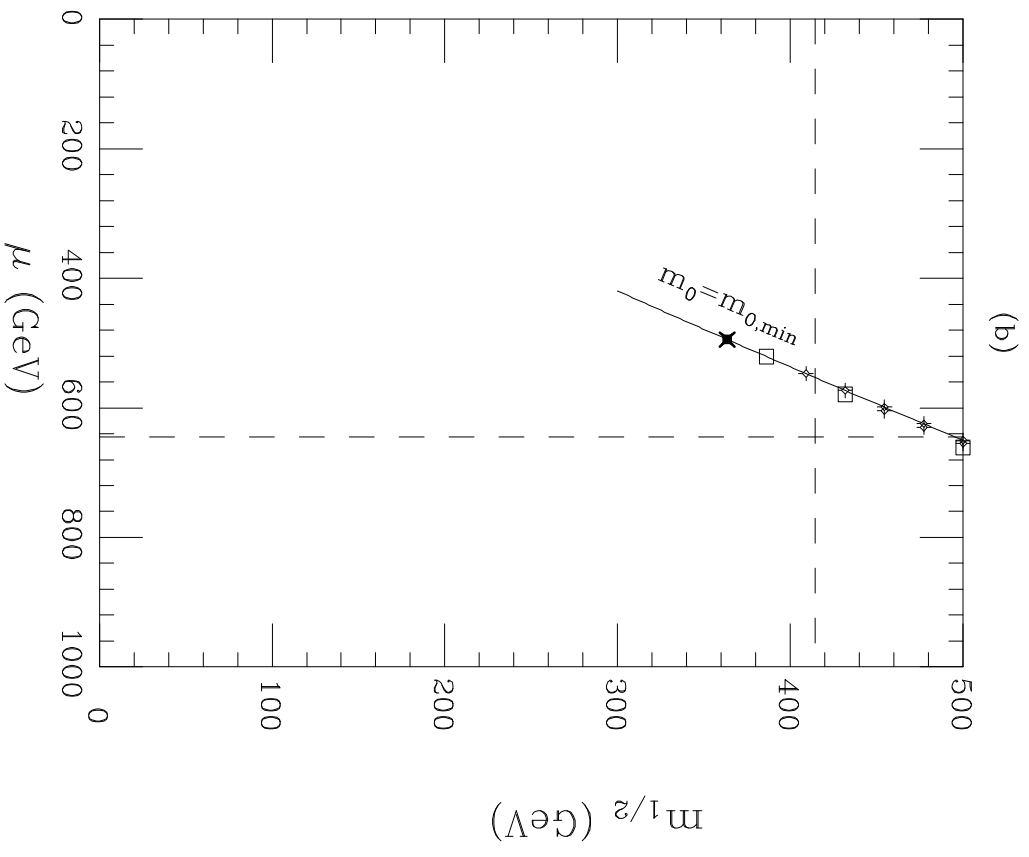
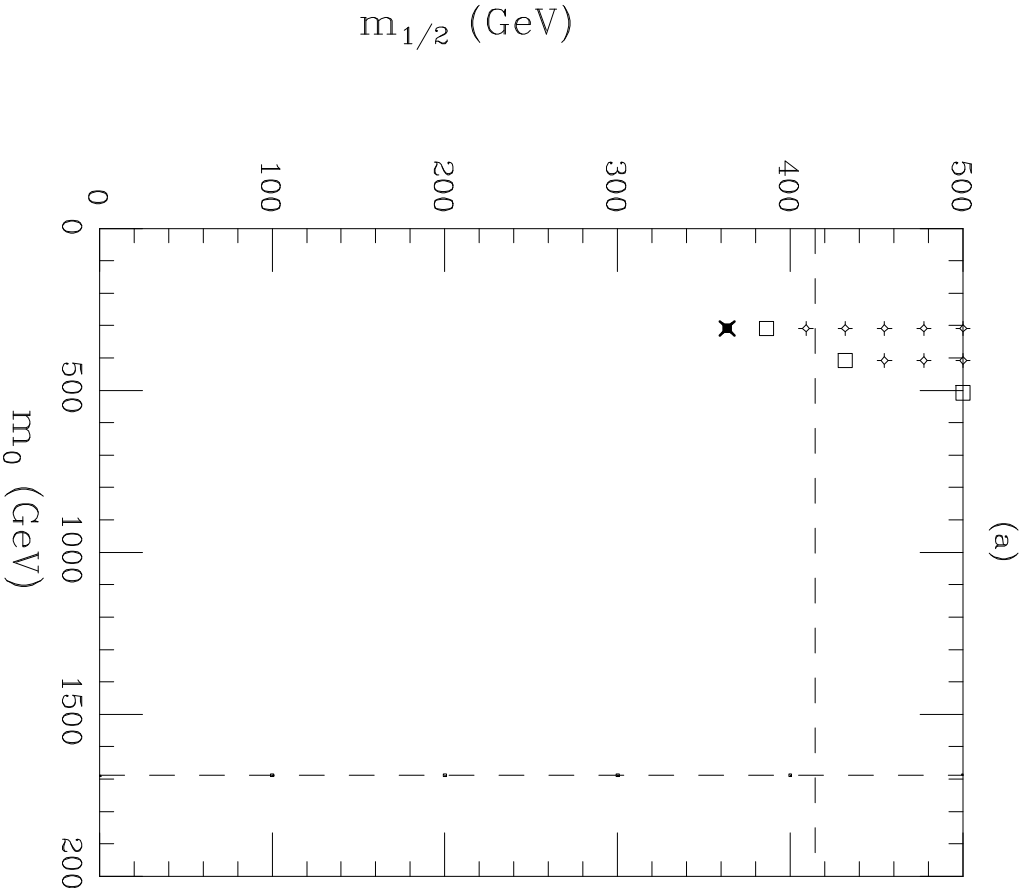


Figure 7

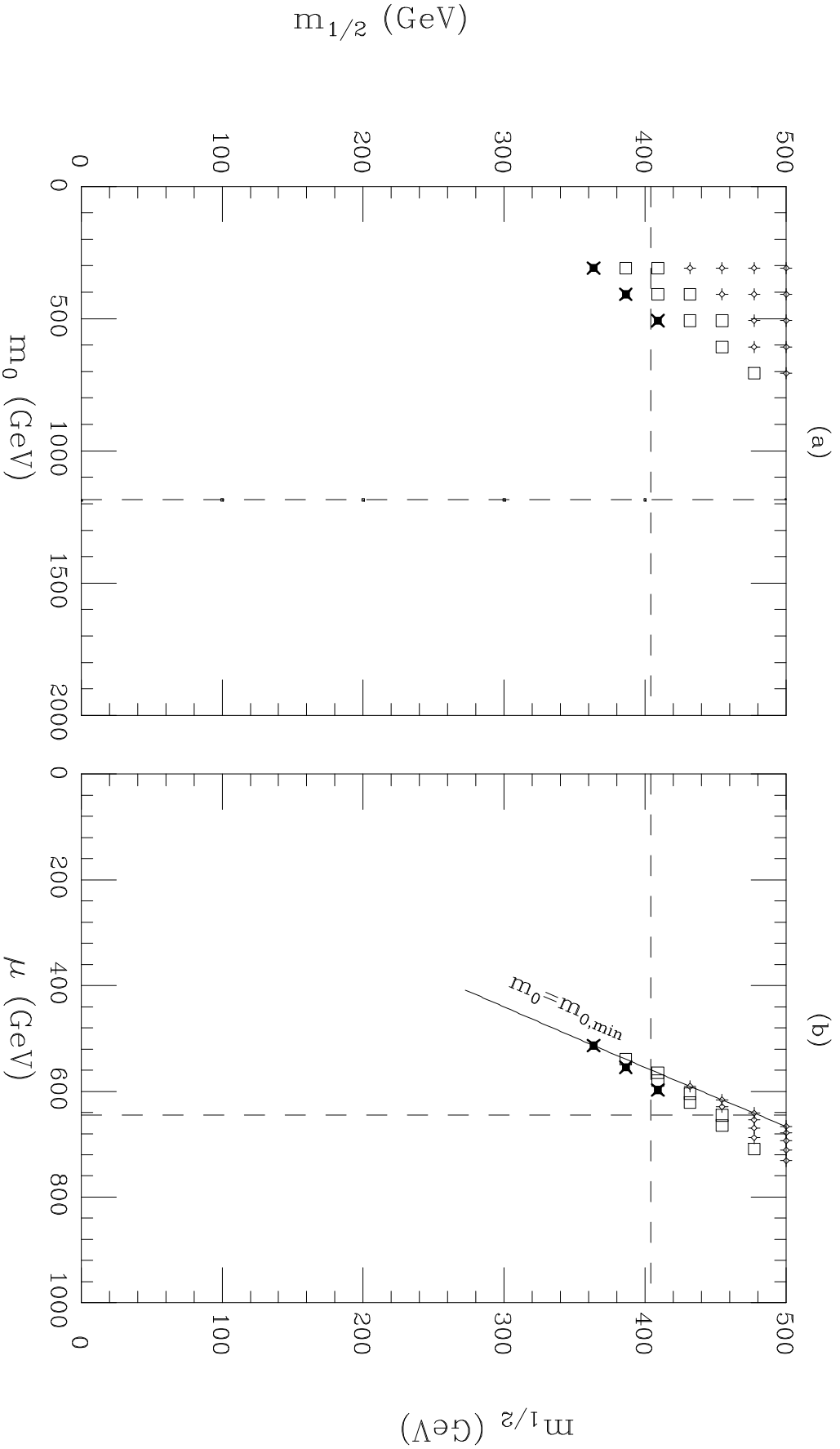


Figure 8

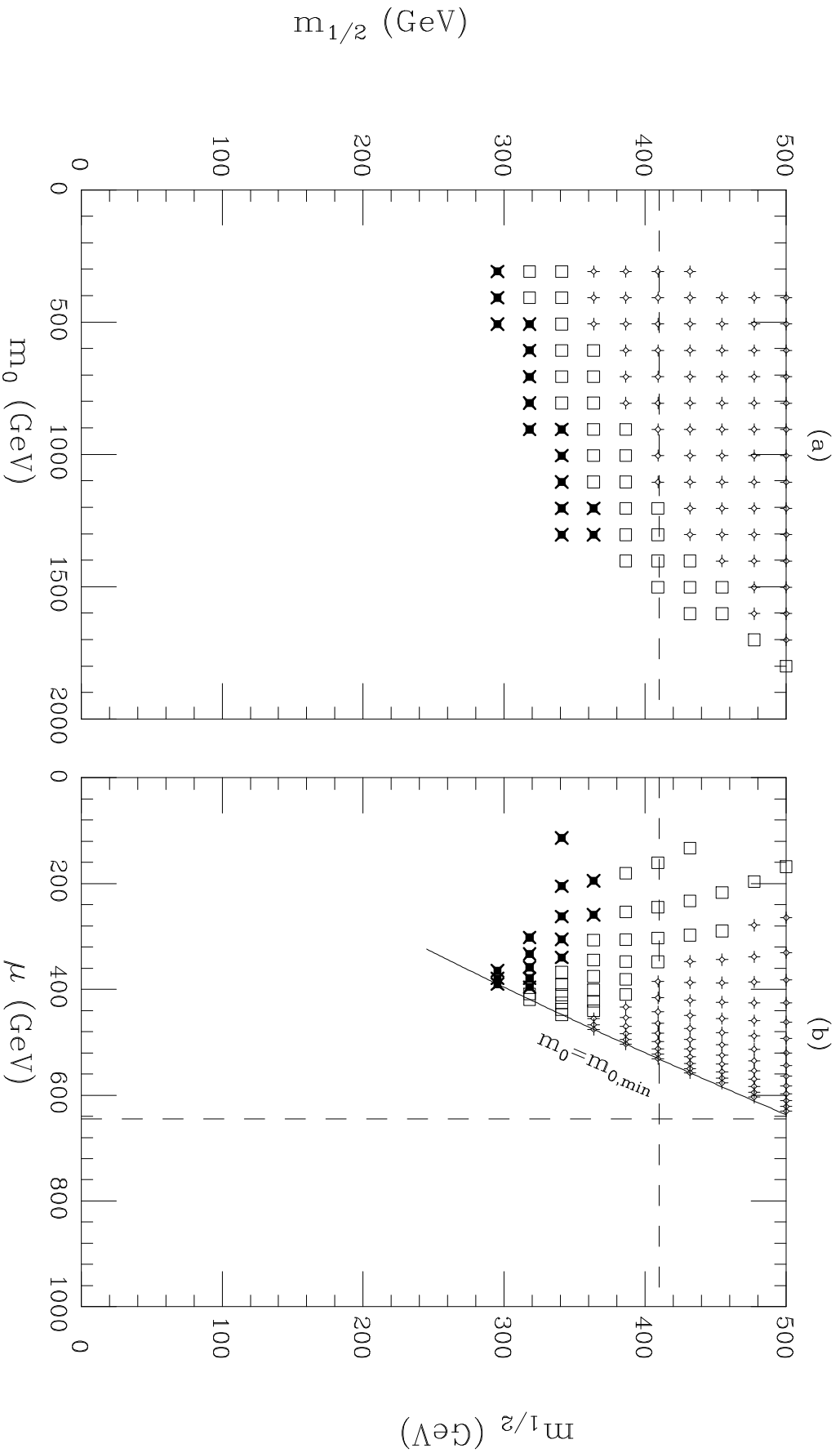


Figure 9

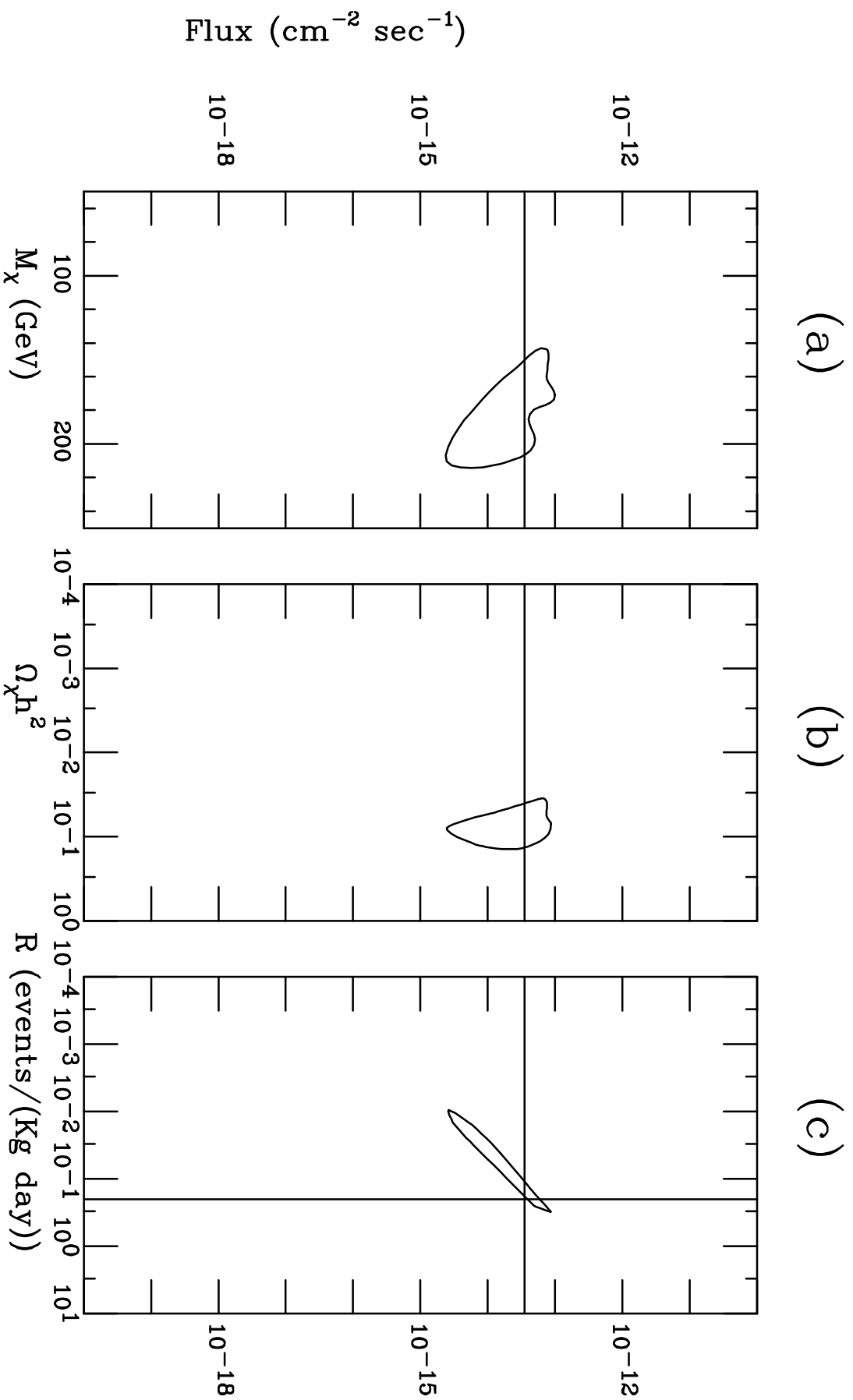


Figure 10

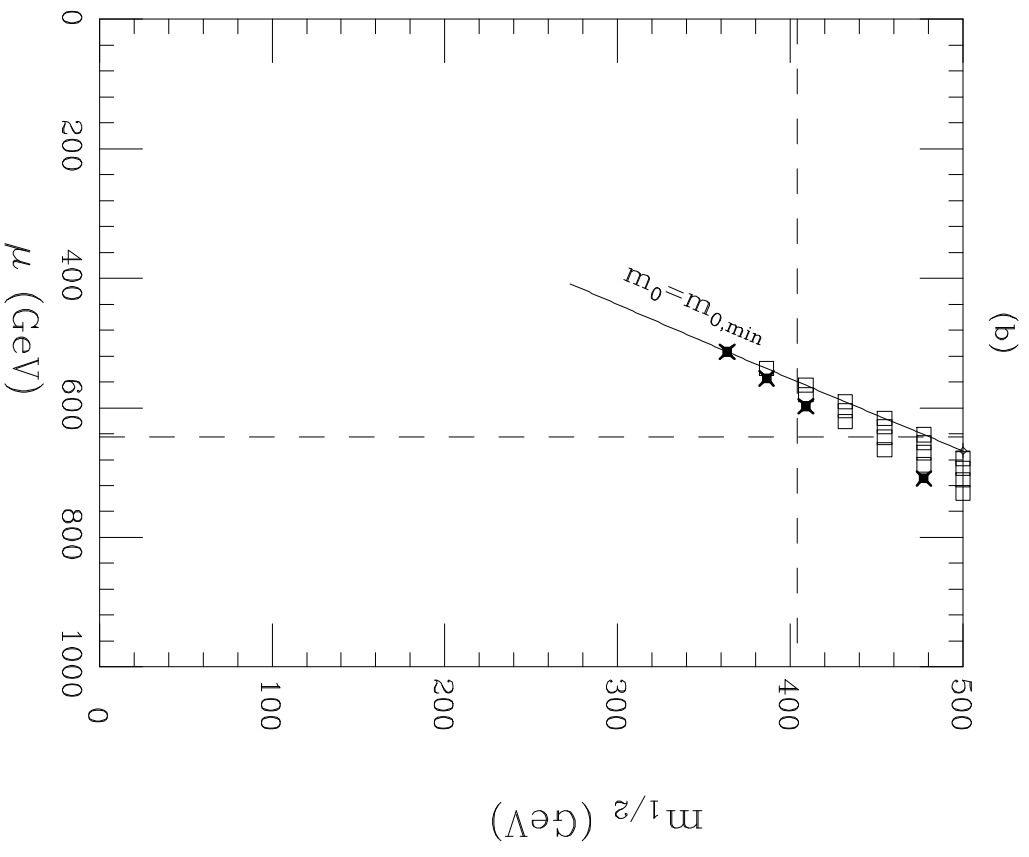
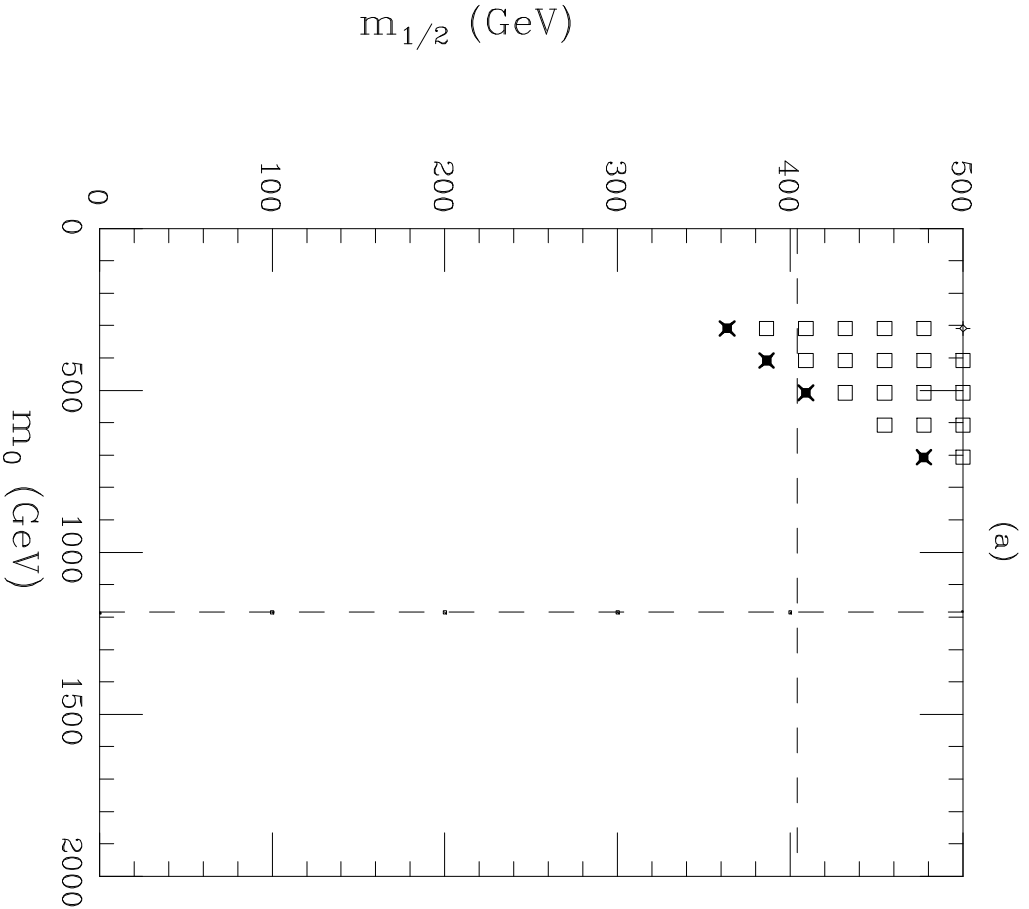


Figure 11